NPL REPORT MAT 141

EXTRACT STRAIN STRESS PARAMETER VIA SPHERICAL INDENTATION, FEA, AND INVERSE MODELLING

LOUISE CROCKER, PIOTR GECA AND HANNAH ZHANG

DECEMBER 2024

Extract strain stress parameters via spherical indentation, FEA and inverse modelling.

Louise Crocker, Piotr Geca, Hannah Zhang

Advanced Engineering Materials

ISSN 1754-2979

DOI https://doi.org/10.47120/npl.MAT141

National Physical Laboratory
Hampton Road, Teddington, Middlesex, TW11 0LW

This work was funded by the UK Government's Department for Science, Innovation & Technology through the UK's National Measurement System programmes.

Approved on behalf of NPLML by
Stefanos Giannis, Science Area Leader – Advanced Engineering Materials

ABSTRACT

A computational study was undertaken to correlate elasto-plastic properties of ductile materials with instrumented indentation test with spherical indenters with radii of 5, 22.5 and 1005 um. Large deformation finite element computations were carried out for different combinations of elasto-plastic properties that covers a wide range of parameters of common pure and alloyed metals: Young's modulus, E was varied from 60 to 210 GPa, yield strength, from 100 to 3000 MPa, with a choice of including strain hardening exponent, n, from 0 to 1. Different kinds of constitutional laws were employed to construct instrumented indentation tests, of which data generated was used for training machine learning algorithm to relate indentation data to elasto-plastic properties of materials.

For the focus of the current report, with restrictions of limited uniaxial experimental data, the results of the simulation of the indentation data carried out with 22.5 µm radius indenter was tested. Nanoindentation results show P91 (a 9%Cr steel) gives a reasonable fit between nanoindentation strain-stress data with tensile results (with the former about 8% lower of yield stress than the tensile test data), while the strain-stress data of Waspaloy (a Ni-based superalloy) is difficult to be extracted from indentation test data. Despite being able to separate initial elastic properties from plastic deformation, the yield stress was much higher (100%) than that measured from the tensile test. This is due to the size effect, which is beyond the scope of the current investigation.

Forward and reverse analysis algorithms were thus established: the forward algorithms allow for the calculation of a unique indentation response for a given set of elasto-plastic properties, whereas inverse modelling algorithms enable the extraction of elasto-plastic properties from a given set of indentation load-displacement data. A representative strain hardening exponent n, and indentation stress factor were identified which allows for the construction of an indentation loading response with experimental tensile strain-stress as input, under Johnson Cook theory. The proposed reverse analysis aims to provide a unique solution of Young's modulus, a representative stress, and the hardening exponent. These values are very sensitive to the experimental scatter, such as materials, indenter radius, contact stiffness and indentation load used.

Given the Johnson Cook law adequately represents the full uniaxial stress-strain response, values of yield stress and hardening factor can be determined for the example cases here on the Waspaloy and P91. However, the plastic properties are very strongly influenced by even small variations in the parameters extracted from instrumented indentation experiments, such as at different loads. Due to the complex strain-stress field under indentation and representativeness of the indentation curve in relation to bulk elasto-plastic properties, it's understood that it's challenging to correlate all the conditions under one case study.

The current study sheds light on the method to extract high resolution strain-stress data via nanoindentation test. For some type of materials that fit a simple work hardening law, experimental methods are capable of extracting yielding stress from a multiple load indentation test, while for some materials such as Waspaloy, it's challenging to correlate nanoindentation strain-stress data with tensile test data. With simulation, it's possible to correlate different models with materials. It must be material-based analysis, there is no single rule that works for all. Therefore, it's important to build up a database, with a range of materials to build a robust simulation model.

CONTENTS

1 INTRODUCTION

Tensile properties of materials constitute the key material specifications needed for structural design, including Young's modulus, yield stress, work hardening rate and ultimate tensile strength. However, to produce conventional tensile testing data, the specimen needs to be available in sufficiently large volumes, which is often not possible, for example for surfaces, inhomogeneous microstructure, coatings, and joints. Indenting the surface with spherical tips with various data analysis procedures has the potential to capture the elastic-plastic response of material, from the initial elastic response during loading to the onset of plasticity and the post-yield behaviour.

Despite the significant progress in the development of test protocols using spherical indenters which has already been achieved, there are challenges when converting load-displacement to indentation stress-strain curves due to the complex stress distribution under an indenter, due to thermal stabilities of test system. For some materials, additional challenges caused by imperfections in the indenter shape make it difficult to evaluate the elastic contact point. Due to the size effect, the representative strains derived from the classic formulations obtained from nanoindentation data, are different from conventional tensile stress strain curves.

For metallic materials with a given set of elastoplastic properties, such as elastic modulus, Poisson's ratio, yield strength, strain-hardening exponent, and tensile strength, an indentation response in the form of a load-displacement curve is produced. The inverse of this should lead to the unique determination of the elastoplastic properties from a set of indentation load-displacement curve. There is a general framework for extracting elastic and plastic properties of engineering alloys through a suite of unique approaches that combine the latest advances in depth-sensing instrumented indentation testing (IIT). In this project, a relationship between the force−displacement curve and the equivalent indentation stress−strain curve will be investigated for P91 (a 9%Cr steel) and Waspaloy (a Ni-based superalloy) in Section 2. These are two type of materials showing different work hardening behaviours.

Inverse modelling is a method that can be used to try to infer bulk material tensile properties from nano- or micro-indentation data. In this case, the finite element analysis (FEA) simulations described in Section 3 have been used to create the data required to train the regression model. At its core, modelling the reverse problem is a multi-output regression problem. The process of feature extraction aims to produce a small number of descriptive features of the observed data. This process should be specific to the data analysed. All features are extracted from the load-displacement curve. Ideally, similar curves should produce similar features to arrive at a stable regression model. Unfortunately, inverse problems are frequently ill-posed and attempts to model them generally lead to numerically unstable predictions, extremely sensitive to the input (load-displacement curves in our case). In Section 4 it is shown that the FEA data generated for training exhibits a lack of uniqueness. Given the limitations, the attempts to train a regression model did not yield satisfactory result at this point. In the interest of understanding this issue in greater depth, we devote more attention to analysis of the features generated in the feature engineering step. These tools should help diagnose the potential issues at an earlier stage.

2 NANOINDENTATION

Instrumented indentation testing (IIT) provides high spatial resolution measurements with little or minimum effort in sample preparation. The use of indentation load-displacement curves has been widely used to correlate microstructure and materials properties at small scale. Routine analysis of the elasto-plastic materials provides reliable Young's modulus and hardness values, however, the compressed stress field under the indenter proves to be difficult to extract stress-strain data from. Numerous efforts have been made including finite element modelling (FEM) and machine learning (ML) to shed light on the developed methods, which are restrained by the limited indentation results at nano- and micro-scale. Another challenge is to correlate available tensile strain-stress data to extracted indentation yield stress values, due to the indentation size effect. A constraint factor is used for both strain and stress parameters to convert indentation to uniaxial tensile stress data.

2.1 EXPERIMENTAL METHOD AND MATERIALS

Efforts have been made to convert load-displacement data to stress-strain curves. Many methods have been suggested and these may or may not include the complete stress-strain curve with an analytical expression. Most IIT methodologies are based on partial unloading and reloading during the test. The "stiffness" of the system, S (in mN/nm), which is given by the load, P, over the penetration depth, h, is evaluated at the points where unloading is carried out. With an increase of indentation depth, h, S increases due to increased volume of material being deformed. Each of these IIT loading and unloading processes is converted to a single point in (true) stress-strain space, which depends on the methods used.

Table 1 provides a list of ways to calculate strain and contact radius. Combinations of the definitions were used to generate indentation strain-stress curves, as shown. The strain-stress plot can vary depending on the method used to calculate contact depth which would be affected by 'pile-ups' or 'sink-ins' of material. This is usually done by obtaining "effective" (or "representative") values of both the stress and the strain acting within the sample at each stage. This would require assumptions, because both stress and strain distribution under an indenter is complex (multi-axial loading situation), unlike uniaxial mechanical tests where equal values are obtained, in addition to the von Mises values of both.

Therefore, correction factors are introduced to better correlate indentation strain-stress to uniaxial mechanical properties. A wide range of analytical formulations have been proposed for obtaining the effective value of stress and strain from indentation testing. The effective strain is commonly taken to be given by the expression originally presented by Tabor,

$$\varepsilon = 0.2a/R_i \tag{1}$$

where a is the contact radius. The factor of 0.2, sometimes termed the "indentation strain constraint factor", is an arbitrary constant, although in fact any kind of averaged (von Mises) strain will not scale linearly with the contact radius during the plastic deformation associated with spherical indentation. Its most appropriate value will vary with the plasticity characteristics of the material. It has often been concluded that, for a good range of metals, this expression is as good as any similar one that might be proposed, although it's certainly true that several other formulations have been put forward as listed in Table 1. The value of contact radius, a, must be obtained experimentally. Traditionally this was done by post indentation scan of the indent. In multi load-unloading processes, this is commonly done via measured values of load, P, indentation depth, h, and system stiffness, S (inverse of compliance, C).

A typical expression for the "contact depth", h_c, is

$$h_c = h - 0.75P/S \tag{2}$$

This represents an attempt to account for the elastic recovery, although clearly the factor of 0.75 depends on the morphology of the indenter tip, which may vary slightly from an ideal sphere.

One way to calculate contact radius is from the contact depth using the standard geometric construction of a spherical cap, giving

$$a = \sqrt{2h_c R_i - h_c^2} \tag{3}$$

This allows the effective strain to be evaluated at each partial unloading point.

The other method is Sneddon's method, based on Hertz contact mechanics formulation for two elastic spheres in contact for the stiffness-based contact radius,

$$a = \frac{S}{2E^*} = (\frac{3PE}{4E^*})^{\frac{1}{3}} \tag{4}$$

where E^* Is the reduced elastic modulus.

Table 1 Summary of ways to calculate contact radius a and indentation strain ε

a / ε	$(\frac{3PE}{4E^*})^{\frac{1}{3}}$	$\sqrt{2h_c R_i - h_c^2}$	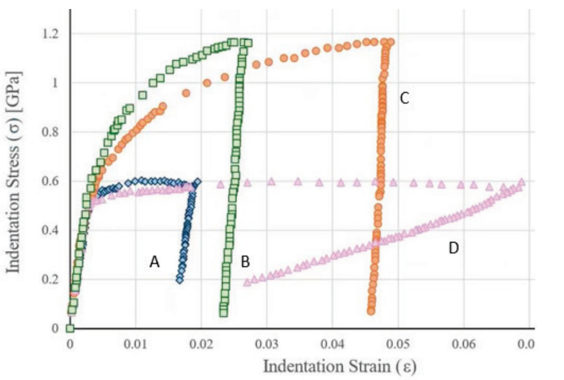
$\frac{4h_t}{3\pi a}$	A	B	
$\frac{4a}{3\pi R_i}$	D	C	

The effective stress is then calculated from indentation hardness. The most common approach is to use the applied load divided by the projected contact area, given by

$$A = \pi a^2 \tag{5}$$

In general, it has been found that simply dividing the load by this area gives an overestimate, so a more common expression is as this

$$\sigma = C\frac{P}{\pi a^2} \tag{6}$$

The constant C is in the range of 2-3 for metallic materials, termed an "indentation stress constraint factor", also indicates a model/material dependent parameter. Various values between about 2.5 and 3 are sometimes employed. As with the indentation strain constraint factor having a value of 0.2, this value of 2.8 was the one originally proposed by Tabor[1] and it also is the one most used.

In the current study, indentation strain related to a/R from most common Tabor equation method C and based on Hertz contact mechanics of method D were used as listed in Table 1, namely indentation method and Sneddon's stiffness method, respectively [2].

2.2 RESULTS

In this section, single and multiple loading and unloading curves obtained from nanoindentation results with spherical indenter of radius of 22.5 μm are analysed and discussed.

2.2.1 Single cycle

The single load-displacement data with different indentation depth/load, and different locations from P91 and Waspaloy are shown in Figure 1. To clearly show the curves, a representative set of indentation curves are given at different loads. Figure 1 (a) shows little change in stiffness (S) – i.e. the unloading gradient with increasing depth appear to be reasonably consistent, indicating stable and rigid test system suitable to avoid over estimation of strain caused by compliance. The maximum penetration ratio (h/R) is about 8% for P91 and 5% for Waspaloy (This ratio gives a very approximate indication of the peak strains within the sample). The strain levels being created in the samples were thus all rather small for both materials.

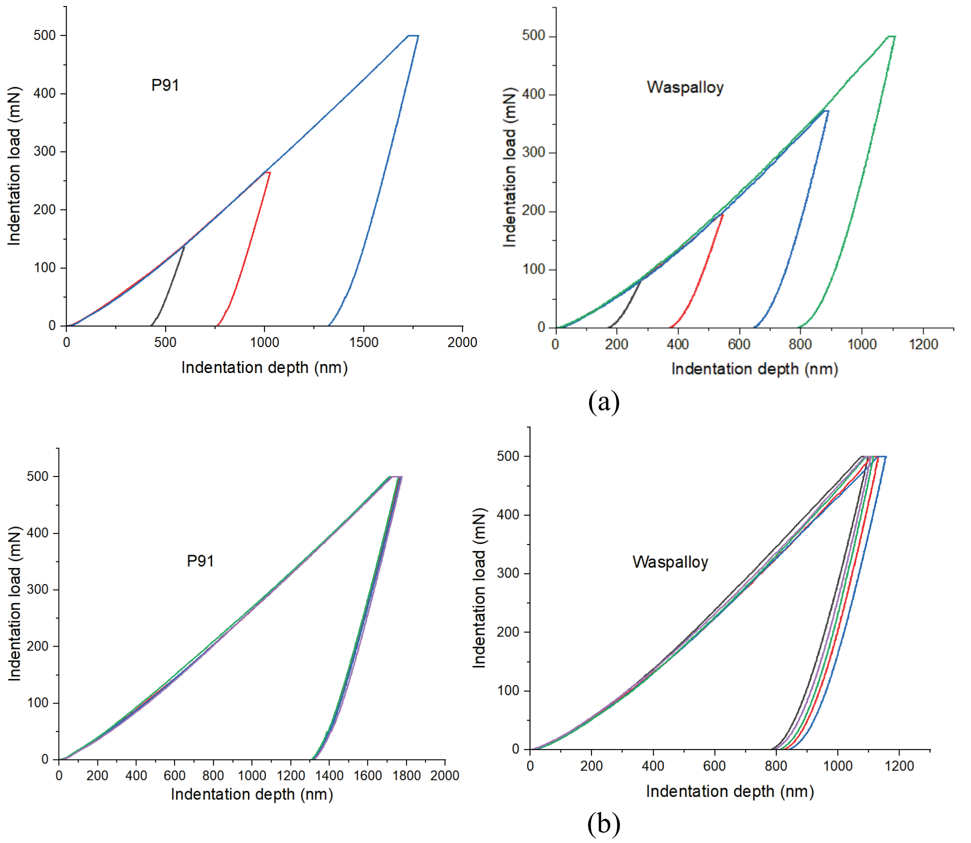

Figure 1 Load-displacement curves of ferritic/martensitic P91 grade steel and Waspaloy at different indentation depths (a) and locations (b).

Figure 1 (b) illustrates the load-displacement data from P91 and Waspaloy from different locations, with indent intervals of 50 μm away from a representative set of indents. According to the unloading indentation depth, the size of indents on Waspaloy is about 10 μm, comparable to the grain size. The diameter of indents on P91 is about 15 µm, which is representative of properties of multigrain. This explains the low variability of load-displacement curves for P91, which are representative of bulk properties of the material, while slightly varied for Waspaloy due to grain orientation effect of about 5%.

2.2.2 Multiload cycle

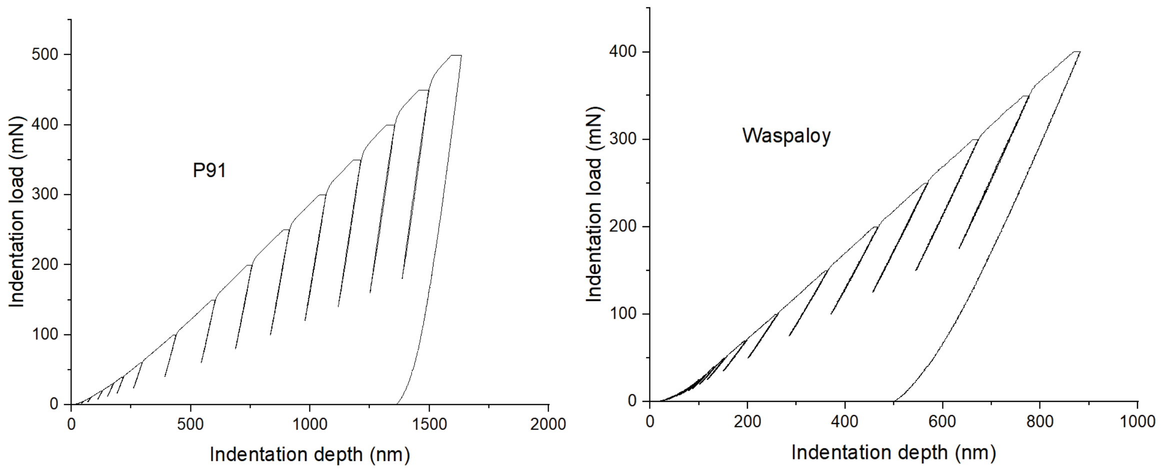

(a)

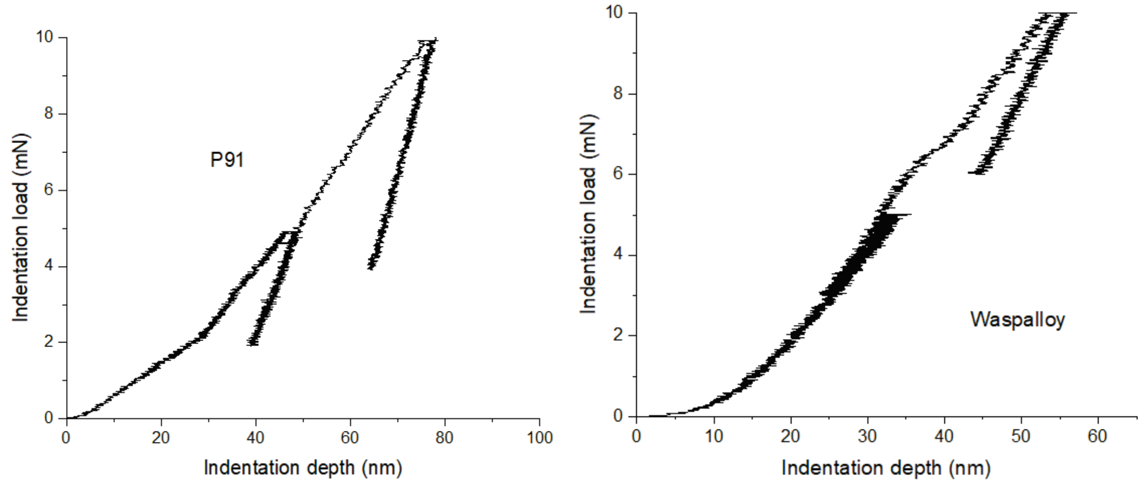

(b)

Figure 2 (a) multiple loading and unloading indentation test on P91 and Waspaloy, and (b) details at initial low load range to observe the elastic to plastic transition.

Multiple loading-unloading indentation curves are shown in Figure 2. The multiple loading curves were made with a 30 second hold at maximum load before unloading, to avoid creep effect to obtain elastic deformation during unloading. The thermal drift of the test system is about 0.05 nm/s. As shown in Figure 2 (a), the displacement of P91 during holding is higher than Waspaloy, indicating that P91 is more subject to creep under indentation stress. To avoid the effect of creep on the extraction of strain-stress data for some metallic materials, i.e. P91, it's recommended to reduce the holding time for future work. Figure 2 (b) shows details of the indentation curves at the initial loading stage. For P91 the plastic deformation starts during the 1st unloading cycle at load of 5 mN; while the loading curve at 5 mN load for Waspaloy is reversible due to pure elastic deformation. The plastic deformation occurs during 2nd loading cycle.

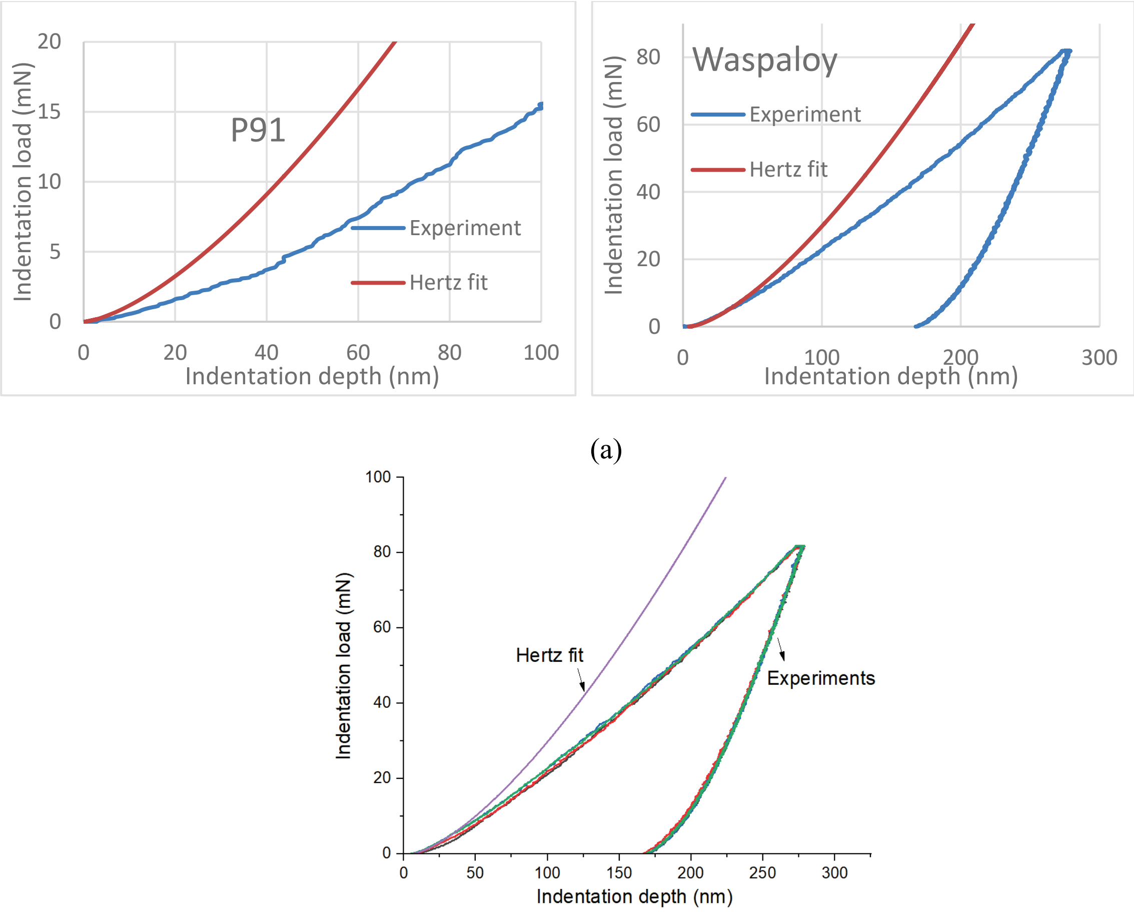

(b)

Figure 3 (a) detect transition from elastic to plastic deformation on P91 and Waspaloy via Hertz contact fitting of load-displacement curves; (b) Hertz fit on different indentation curves to show the representative value of yield load on Waspaloy.

Figure 3 illustrates the transition from elastic to plastic deformation in these typical elasto-plastic deformation metallic materials, by comparing with elastic Hertz contact.

$$P = \frac{4E^{*}\sqrt{R}h^{m}}{3} \tag{7}$$

Here m is the geometrical parameter, for a perfect sphere it's 1.5. Due to the imperfection of the indenter tip, m of 1.45 was used to generate the best fit.

The Hertz fit was used for both P91 and Waspaloy on different indentation curves at different locations. It's not possible to identify the overlap or find the elastic loading region in P91, indicating it is easier to yield compared with Waspaloy, as shown in Figure 3 (a). Figure 3 (b) shows consistency of the original elastic loading at load of about 6 N, on a range of indentation curves at maximum indentation depth of 300 nm.

It's noticed that with increasing indentation depth, the variation on indentation load-displacement starts to occur at maximum indentation depth of 400 nm on Waspaloy, as shown in Figure 1 (b), below which indentation curves at different locations overlaps as shown in Figure 3 (b). This indicates anisotropic (or grain orientation related) work hardening behaviour in Waspaloy, which have been studied but not a focus of this work.

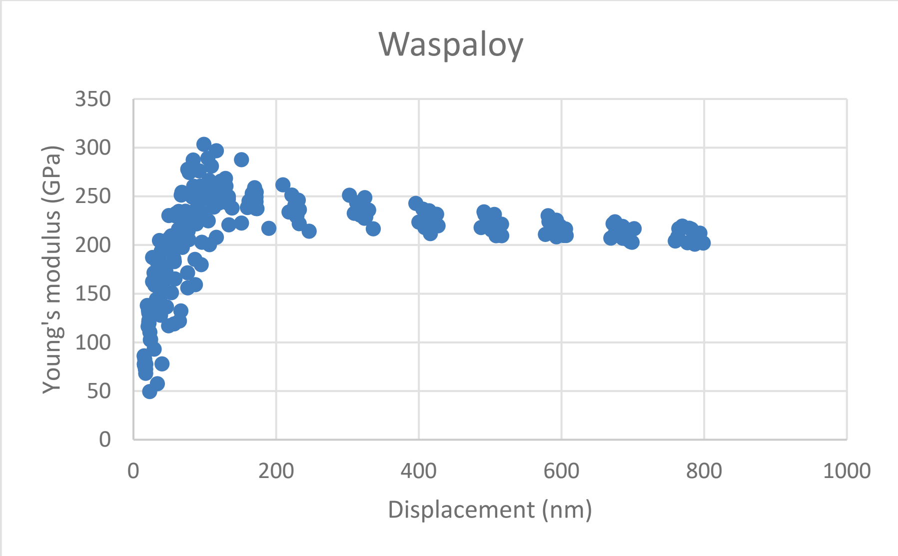

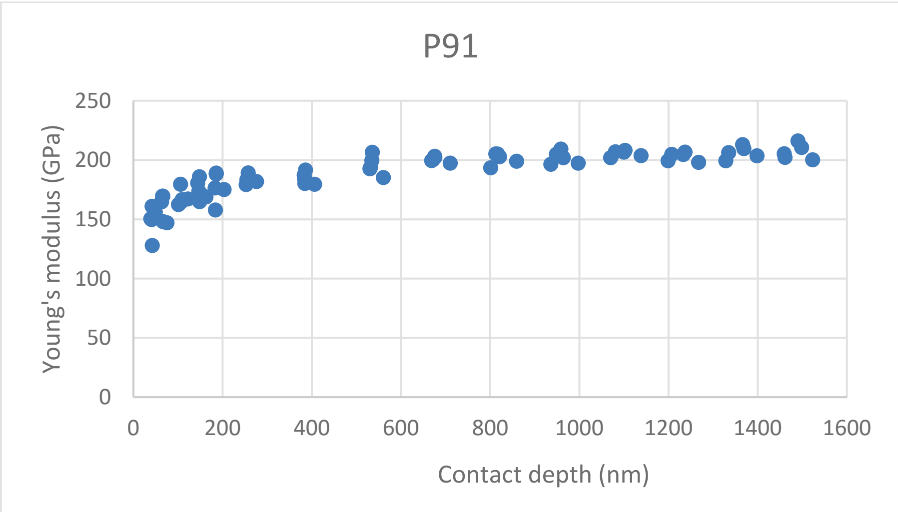

Figure 4 Young's modulus values of Waspaloy and P91 from multiple loading and unloading nanoindentation test as a function of indentation depth.

Figure 4 shows the Young's modulus values obtained from multiple load-displacement curves for both materials, of which the Young's modulus values are consistent with indentation depth after maximum indentation depth of 400 nm. They are about 225 and 205 GPa for Waspaloy and P91, respectively, these values are consistent with experimental tensile test results.

2.2.3 Strain-stress analysis

For the conversion of indentation strain and stress to tensile strain stress by introducing constraint factors, all the current existing model assumes that the materials can be accurately described by the Hollomon power law work-hardening relationship, as

$$\sigma = K\varepsilon^n \tag{8}$$

The tensile strain-stress curve for Waspaloy is shown in Figure 5, the difference between engineering and true values of stress and strain is small [3]. In the region with comparable strain range with nanoindentation, the work hardening law (eq. (8)) does not generate a good fit with tensile results, as $\sigma = 865\varepsilon^{0.075}$. According to this relationship, the yield stress computed is about 535 MPa from nanoindentation Sneddon's stiffness equation, which is much lower than the experimental tensile values.

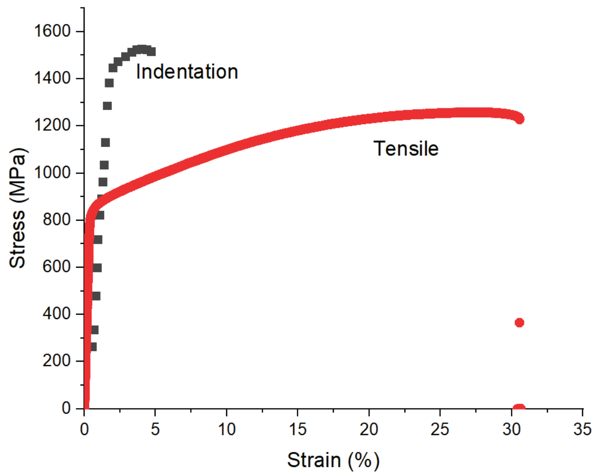

(a)

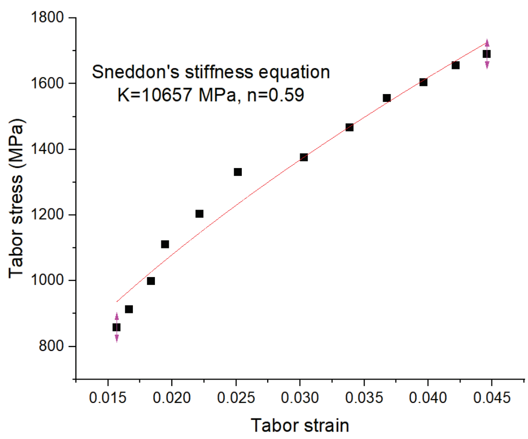

(b)

Figure 5 Strain-stress data for Waspaloy obtained from (a) tensile testing and Tabor indentation calculation; (b) Sneddon's stiffness equation.

According to Hertz contact, the maximum shear stress is reached at 0.5a of indentation depth,

$$\tau_{max} = C(\frac{6PE^{*2}}{\pi^3 R^2})^{1/3} \tag{9}$$

for materials with Poisson's ratio of 0.3, C is 0.31, E^* is reduced Young's modulus, R is the radius of the indenter, P is the load where plastic deformation occurs. For Waspaloy, it's constant that the yield occurs at load of 6 ± 0.15 mN. The calculated maximum shear stress is about 1.41 GPa. As there is little crystal orientation effect observed in current test results, it indicates that the deformation occurred attributed to the same mechanism. This stress is much higher than tensile yield stress of about 819 MPa, in current work, the mechanism behind this is not clear.

According to previous research [4], Grade 91 steels can be considered power-law hardening materials, so the plastic segment of the tabor stress calculated from indentation strain stress (as shown in Figure 6) is fitted to the simple constitutive equation. This continuity at the point of yielding requires:

$$K = \sigma_y (\frac{E}{\sigma_y})^n \qquad (10)$$

Figure 6 (a) shows strain stress data from tensile testing and Tabor indentation data and (b) Tabor indentation data according to Sneddon's stiffness equation. The best fit was given by Sneddon's stiffness fitting, giving K and n of 1724 MPa and 0.22, respectively, the yield stress is 456 MPa (495 MPa from tensile test) according to the above equation. This value is about 8% lower than tensile stress data, while the values are close to literature data obtained with an indenter with a radius of 20 µm [4]. A summary of the extracted parameters are given in Table 2

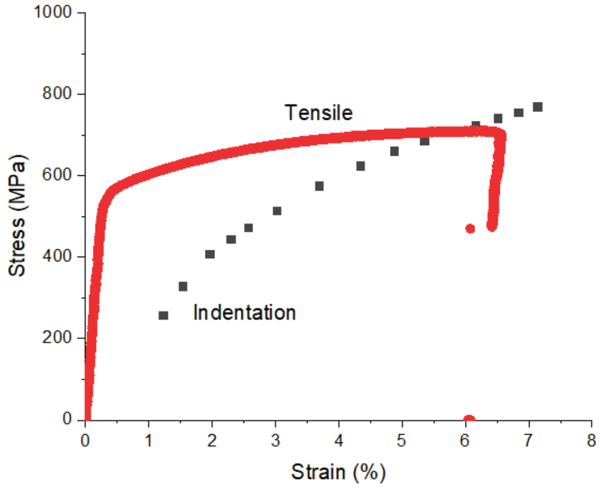

(a)

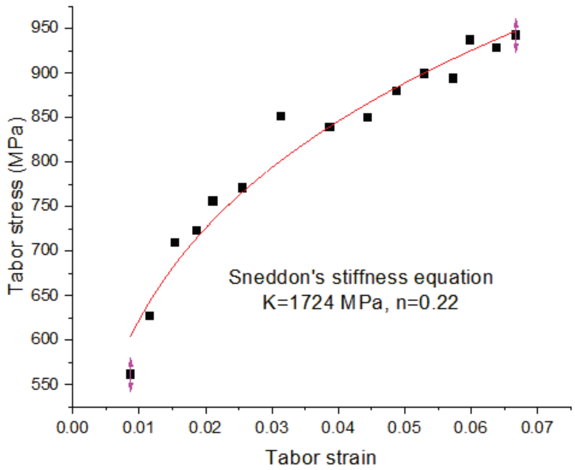

(b)

Figure 6 Strain-stress data for P91 obtained from (a) tensile testing and Tabor indentation calculation; (b) Sneddon's stiffness equation.

Table 2 Summary of strain-stress parameter extraction from nanoindentation data from P91 and Waspaloy.

	Power law work hardening				Hertz
	E* (GPa)	K (MPa)	n	σ_y (MPa)	τ_{max}(MPa)
P91	193	1724	0.22	456	N/A
P91 Tensile	193	940^	0.098	495	
Waspaloy	203	N/A			1408
Waspaloy Tensile	203			819	

^data from literature [4]

2.3 SUMMARY OF NANOINDENTATION EXPERIMENT

Single and multiple nanoindentation with a spherical indenter of radius 22.5 µm were carried out on P91 and Waspaloy. The results show that the current indenter size gives uniformity of indentation curves, indicating the representative properties of bulk materials; while for the Waspaloy, there is a size effect shown via increasing indentation depth, where a different work hardening response was observed. The traditional measurement of indentation modulus is consistent with tensile properties for both materials.

It's not possible to separate elastic deformation from initial loading in P91 with the current indentation radius, while initial elastic deformation in Waspaloy under the nanoindenter was captured and separated from the load-displacement curve via elastic Hertz contact mechanism.

Several methods were used and analysed to obtain extra strain-stress data from multiple load-displacement curves. For P91 and Waspalloy, tabor strain and stress with strain related to a/R were found to work better with current experimental settings. The results demonstrate that it's challenging to make meaningful measurements of yield strength with existing models and to convert the indentation strain, stress date to Tabor strain stress for Waspaloy, while the Young's Modulus and yield stress data collected from the P91 fit reasonably well to experimental tensile data. This was attributed to that P91 fit work hardening law, which is the assumption of the indentation models.

For Wasploy, via Hertz fit, the initial maximum shear stress was calculated to be about 1.4 GPa, which is much higher than the tensile yield strength. This has been shown to be the case from other indentation measurement methods, therefore, a more complex model should be developed to be representative of the complex work hardening behaviour of Waspaloy.

3 FEA OF INDENTATION

FEA (finite element analysis) is a useful tool to generate predictions of the behaviour of a material for a defined set of material parameters. This ability has been utilised, though a parametric study, to generate a series of predicted indentation load-displacement curves for given ranges of material parameters with the aim of producing training data for a neural network.

3.1 GENERATION OF BASE FE MODEL

A finite element (FE) model was generated using the FE software Abaqus CAE [5] to predict the behaviour of an indentation experiment where a 22.5 µm radius indenter indents into a block of material. An axisymmetric implicit model with geometric non-linearity was selected as a suitable representation of the system. The indenter was represented by an analytical rigid surface with a reference node to control movement.

The sample was 100x100 μm and the indenter was positioned at the surface of the sample along the symmetry axis. The sample geometry was partitioned to create a region, 50x20 μm, directly below the indenter. This allowed a refined mesh to be defined in the area of contact. The geometry was meshed mainly with axisymmetric solid 4-node bilinear, reduced integration elements with hourglass control, with some 3-noded elements used to facilitate moving from a very refined mesh to a coarser mesh in the bulk of the sample. The element side length in the refined mesh region is 0.333 μm. Figure 7 shows the partitioned region with axis of symmetry on the left (a), the full meshed geometry (b) and refined mesh area (c). Mesh sensitivity analyses were carried out to confirm that this was a suitable mesh refinement balancing accuracy of predictions against computational runtime. Runtime was especially important as this model was to be used for parametric analyses; any improvements in runtime leads to a big computational saving when running hundreds of analyses. Sensitivity checks were also carried out on the size of the refined region to make sure that the edges of this region didn't constrain the stress and strain predictions in any way.

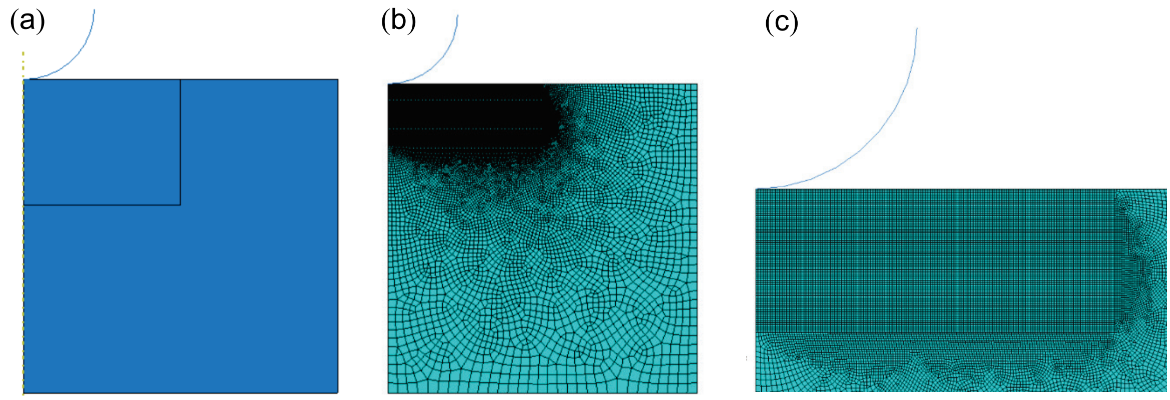

Figure 7 Geometry of the FE indentation model (a), meshed geometry (b) and refined region (c).

Surface to surface contact was defined between the outer surface of indenter and the top surface of the refined region in the sample. Friction (μ = 0.05) is included in the contact definition. A spring is attached to the indenter reference node and a small value of spring stiffness was applied.

Constraints were applied to the outer edges of the geometry, and the reference node of the indenter was constrained to allow movement in the vertical direction only. Two analysis steps were created. Firstly, a displacement is applied to the reference node of the indenter to move the indenter downwards vertically to indent the substrate and then in the second step the indenter is moved upwards, back to its starting location. This approach is in contrast to the experimental test where a fixed load is applied to the indenter but in FEA, better convergence is achieved by applying displacements. In this case, the displacement applied was the maximum displacement obtained from the experimental data, corresponding to the maximum applied load.

3.2 MATERIAL DEFINITIONS

3.2.1 Material Models

A range of material models are available in Abaqus to represent the behaviour of the materials in an analysis. The materials considered in this work were Waspaloy (a nickel-based superalloy) and P91 (a Steel alloy). Both these materials exhibit elastic-plastic material behaviour. One way to introduce the effect of hardening due to plasticity is to use a von Mises elastic-plastic model including a hardening curve obtained from experimental tensile data. The derivation of this is detailed in Section 3.2.2 below.

In previous indentation modelling work, material behaviour was represented by an elastic-perfectly plastic material model, where only the Young's Modulus, Poisson's ratio and Yield stress were provided, and the Young's Modulus and yield stress were the parameters varied in the parametric study. To improve predictions of material behaviour in the current analyses, full representation of the hardening behaviour was used. As the aim of this work is to use parametric analyses to obtain predicted behaviour from indentation into a sample with a range of material properties, use of a single hardening curve was not ideal. Hence alternative models, with hardening behaviour defined by analytical equations, were also investigated. These are described in Section 3.2.2 below. The material parameters for the P91 material are detailed in Section 3.2.3.

3.2.2 Waspaloy Material Properties

A single experimental tensile stress-strain curve was obtained for the Waspaloy material, see Figure 8, and used to calculate the Young's Modulus and plasticity hardening curve for use in the von Mises material model. Without multiple tensile stress-strain curves, it is not possible to gauge how representative of the bulk material this curve is.

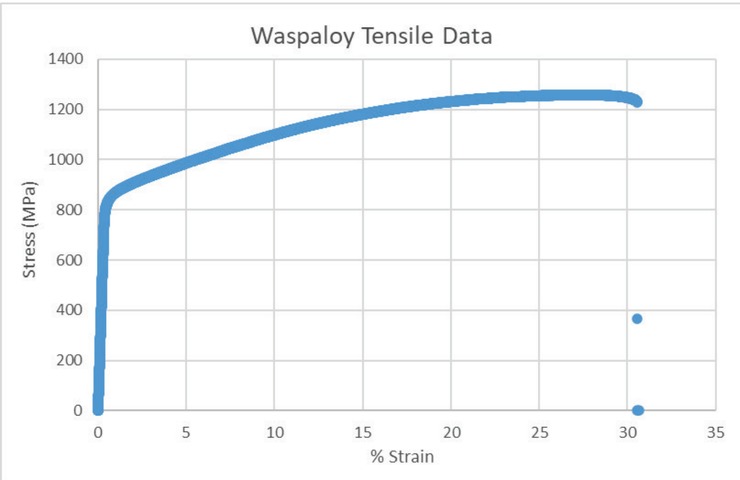

Figure 8 Experimental tensile stress-strain curve for Waspaloy.

The Abaqus FE software requires the hardening curve to be defined in terms of true stress-true plastic strain [5] using the following equations:

$$\varepsilon_T = \ln(1 + \varepsilon) \tag{11}$$

$$\sigma_T = \sigma \exp(\varepsilon_T) = \sigma(1 + \varepsilon) \tag{12}$$

$$\varepsilon_T = \varepsilon_T^e + \varepsilon_T^p \tag{13}$$

$$\varepsilon_T^p = \varepsilon_T - \varepsilon_T^e = \varepsilon_T - \frac{\sigma_T}{E} \tag{14}$$

The hardening curve is then defined from the point that the true plastic strain first becomes increasingly positive, with the stress at this point being the material yield stress. A reduced set of data was selected from the full true stress-true plastic strain curve to represent the hardening curve within Abaqus, see Figure 9.

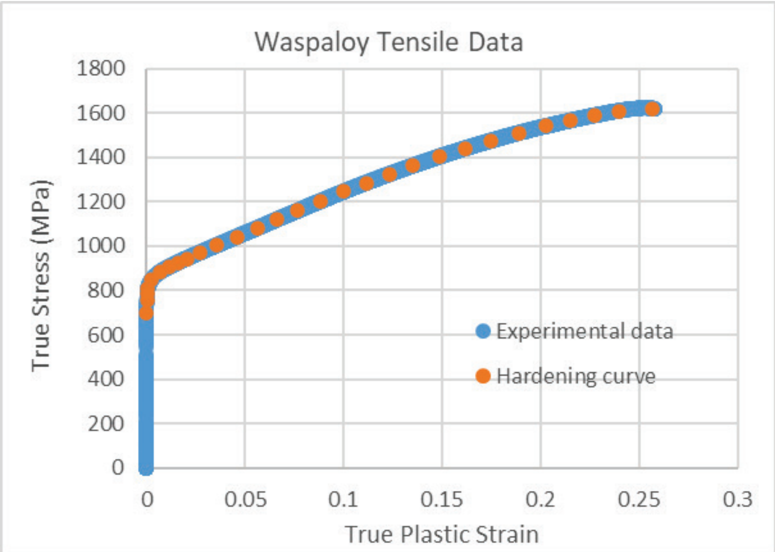

Figure 9 Waspaloy hardening curve plotted on True Stress – True Plastic Strain data.

The validity of this data was confirmed by running a single unit cell analysis i.e. one element constrained to allow tensile loading. Figure 10 shows that this elastic-plastic model accurately represents the tensile behaviour of this material.

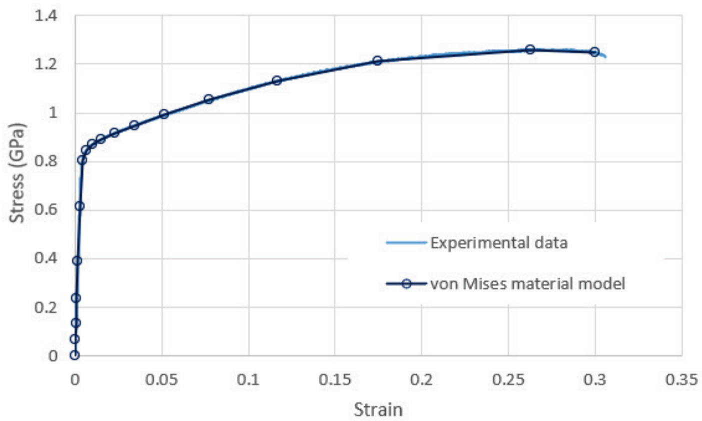

Figure 10 Comparison between experimental tensile stress-strain data and the tensile behaviour predicted using von Mises elastic-plastic model.

Although this material model represents the Waspaloy tensile deformation well, it is not suitable for use in parametric analyses where the aim is to sweep across a range of material behaviours. For this reason, an alternative model is required where the hardening behaviour is defined by analytical equations with parameters that can be varied across defined ranges to provide a set of training data for use in a neural network.

Two different models available in Abaqus were explored. These were the Johnson-Cook model and the deformation plasticity model. The deformation plasticity model gave a poor representation of the experimental behaviour, so will not be reported here.

The Johnson-Cook model is a particular type of Mises plasticity model with analytical forms of the hardening law, as well as rate and temperature dependence if required. The material behaves as linear elastic when the stress is below the yield stress. At higher stresses, the relationship for describing the static true yield stress, σ^0, is:

$$\sigma^0 = \left[A + B\left(\bar{\varepsilon}^{pl}\right)^n\right]\left(1 - \hat{\theta}^m\right) \tag{15}$$

Where $\bar{\varepsilon}^{pl}$ is the equivalent true plastic strain and A, B, n and m are material parameters. $\hat{\theta}$ is the non-dimensional temperature. As temperature effects are not included in the analysis, this term can be omitted, so only the parameters A, B and n are required to describe the hardening behaviour.

The parameter A is the yield stress of the material. Equation (15) was rewritten as:

$$\ln(\sigma - A) = n.\ln\left(\bar{\varepsilon}^{pl}\right) + \ln B \tag{16}$$

The parameters B and n were obtained from plotting $\ln(\sigma - A)$ against $\ln\left(\bar{\varepsilon}^{pl}\right)$, whereby n is the slope of the linear portion of the plot and $\ln B$ is the intercept.

There are several options for defining the yield stress, parameter A. It can be the yield stress calculated when obtaining the hardening curve described above, where selection of the stress value at which the plastic strain becomes consistently positive is slightly arbitrary. When there isn’t a clearly defined yield point, an offset yield stress can be used, this corresponds to a point at the intersection of a stress-strain curve and a line which is parallel to the linear portion of the stress-strain curve but offset by a small increment of strain.

The two methods outlined above produce different sets of parameters, see Table 3.

Table 3 Waspaloy Johnson-Cook parameters.

Johnson-Cook parameters	E (GPa)	A (GPa)	B (GPa)	n
Yield from hardening curve	**226.59**	**0.6990**	**2.2204**	**0.6234**
Using offset yield	226.59	0.8041	2.7034	0.8093

These two sets of parameters were used in single element analyses to assess predictions of the tensile stress-strain material behaviour and also in indentation analyses to assess the ability to predict the load-displacement behaviour. The single element analysis, Figure 11, shows that the analysis run using the A parameter obtained from the hardening curve yield stress fits the experimental data well at high strains but doesn’t fit in the initial early plastic region. The analysis run using the A parameter obtained from the offset yield stress fits the experimental data well until high strains are reached.

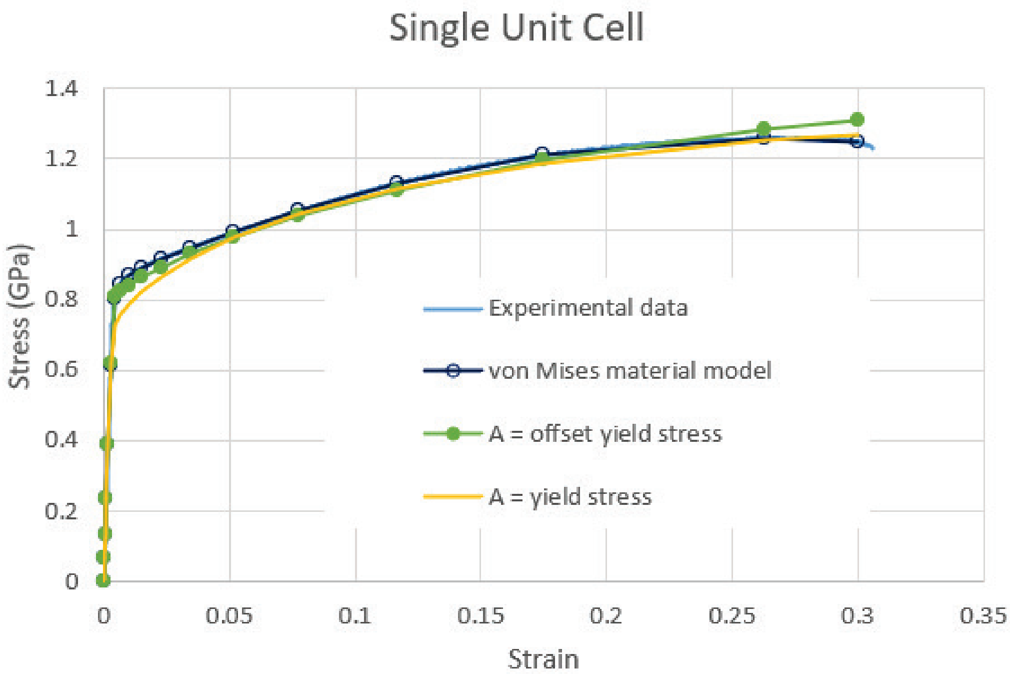

Figure 11 Experimental stress-strain data compared with predictions from the von Mises model and the Johnson-Cook model run with the two different parameter sets in single element tensile analyses.

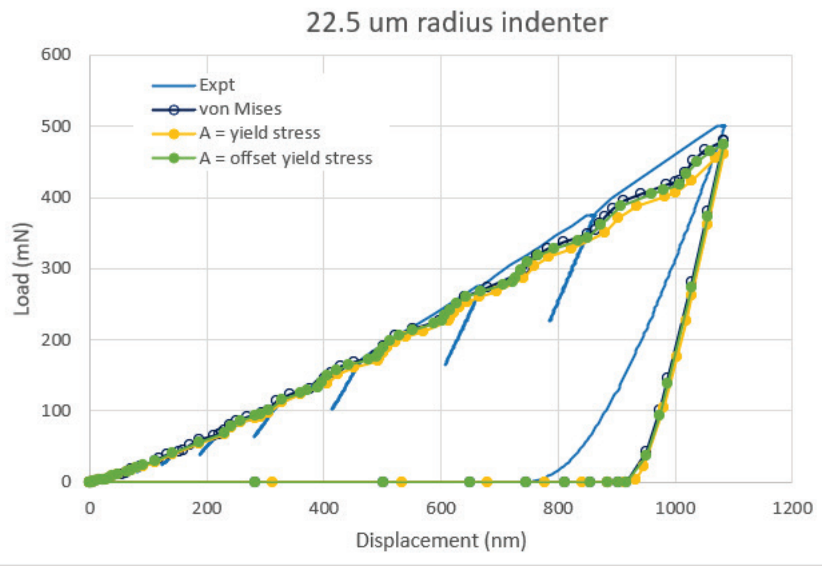

Figure 12 Experimental indentation data compared with predictions from the von Mises model and the Johnson-Cook model run with the two different parameter sets.

The indentation results in Figure 12 show very little difference in predicted load-displacement response between the two different models using the two sets of Johnson-Cook parameters. One thing that is clear is that an applied displacement of 1083 nm doesn't quite predict the expected load of 500 mN, and that the unloading curve is does not align with the experimental unloading data.

Due to the higher hydrostatic pressure under the indenter and the constraint of the surrounding elastically deforming material, the indentation yield strength is known to be higher than the uniaxial yield strength. The correlation between the two is referred to as the Tabor factor. This factor can be used to reassess the Johnson-Cook material parameters, as the parameter A represents the yield stress. Assuming a Tabor factor of 3, the Johnson-Cook parameter A was increased by a factor of 3, see Table 4, resulting in an increase in the predicted load in the analysis. Experimentally the indenter is loaded to 500 mN, so the predicted load was then scaled to this value. Figure 13 shows the data from this analysis compared to the experimental data. The predicted load-displacement curve with the load recalibrated to 500 mN produces a good correlation with the experimental data in both the loading and unloading regions.

Table 4 Waspaloy Johnson-Cook parameters using A increased by a factor of 3.

Waspaloy	E (GPa)	Calc A (GPa)	3*A (GPa)	B (GPa)	n
Johnson-Cook parameters	226.59	0.8041	2.4123	2.7034	0.8093

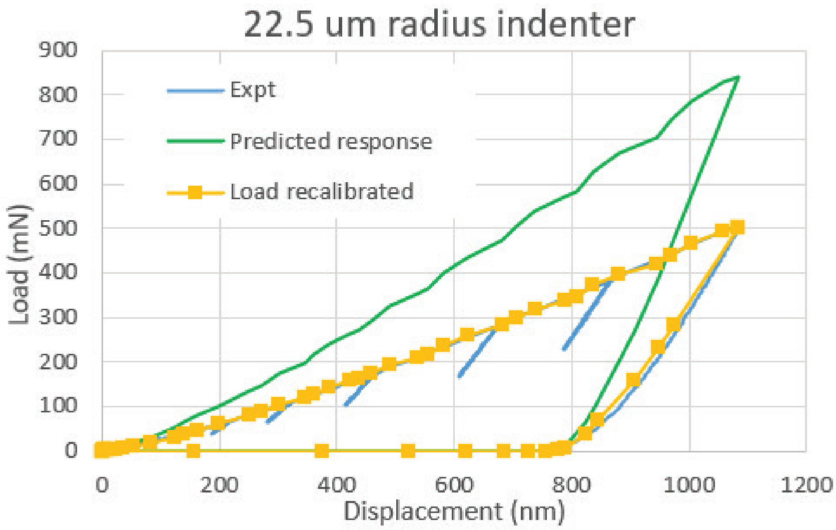

Figure 13 Experimental data compared to predicted load-displacement response from analysis with yield stress (A parameter) increased by a factor of 3 and the same data recalibrated to a load of 500 mN.

3.2.3 P91 Material Properties

A single experimental tensile stress-strain curve was obtained for the P91 material, see Figure 14, and used to calculate the Young's Modulus and plasticity hardening curve for use in the von Mises material model, see Figure 15. Without multiple tensile stress-strain curves, it is not possible to gauge how representative of the bulk material this curve is.

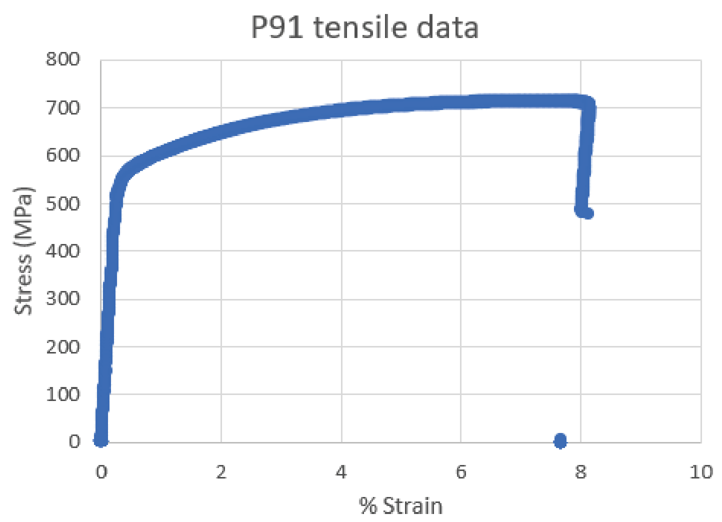

Figure 14 Experimental tensile stress-strain curve for P91.

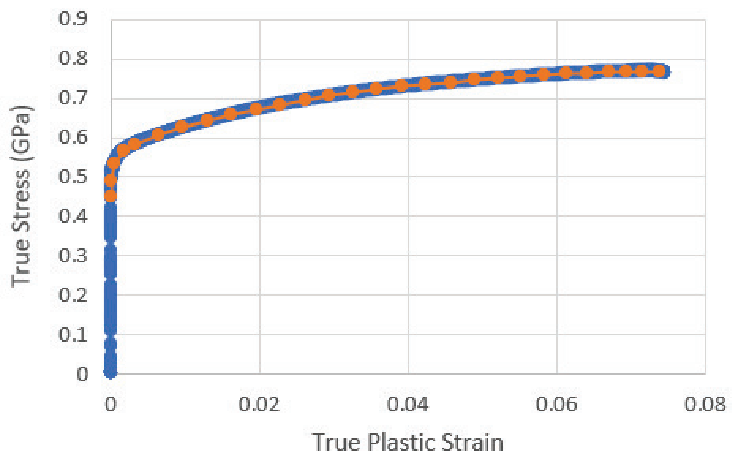

Figure 15 Hardening curve overlaying P91 experimental tensile true stress-true plastic strain data.

The derivation of P91 Johnson-Cook material parameters was conducted in the manner described in Section 3.2.2 with the parameters presented in Table 5.

Table 5 Calculated P91 Johnson-Cook parameters.

P91	E (GPa)	A (GPa)	B (GPa)	n
Johnson-Cook parameters	211.46	0.4956	0.9772	0.4604

Both the von Mises and Johnson-Cook material models were used in single element analyses to assess predictions of the tensile stress-strain material behaviour and also in indentation analyses to assess the ability to predict the load-displacement behaviour.

The single element analysis (Figure 16) shows, as expected, that the analysis run using von Mises fits the experimental data very well. The analysis run using the Johnson-Cook model fits the experimental data well until high strains are reached.

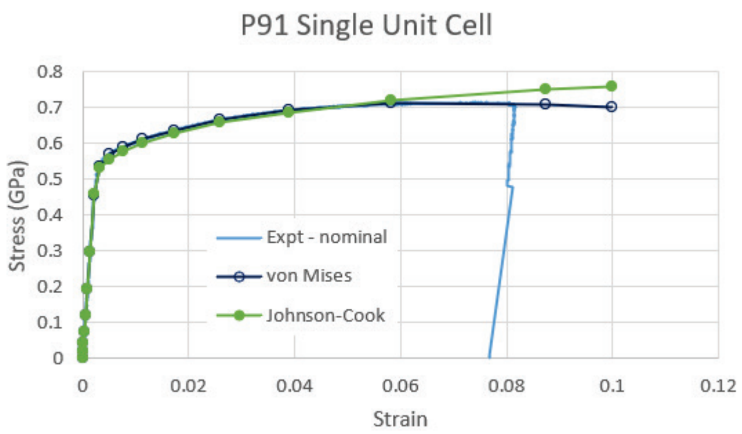

Figure 16 Experimental stress-strain data compared with predictions from the von Mises model and the Johnson-Cook model in single element tensile analyses.

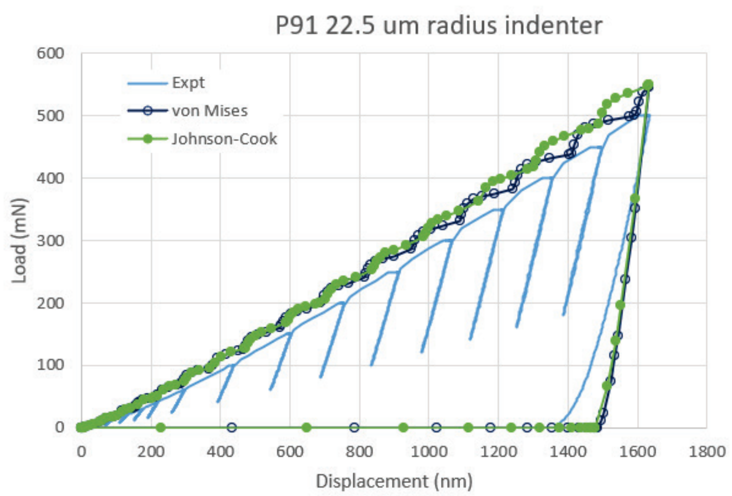

Figure 17 P91 experimental indentation data compared with predictions from the von Mises model and the Johnson-Cook model.

The indentation results in Figure 17 show very little difference in predicted load-displacement response between the two different models. The applied displacement of 1634 nm (obtained from the experimental data) predicts a load that exceeds the expected load of 500 mN. Once again, as was the case with the Waspaloy predictions, the unloading curve does not align with the experimental unloading data. Hence a Tabor factor of 3 was used to adjust the A parameter to 1.4868 GPa. The resulting prediction is shown in Figure 18, along with the curve obtained when the data is recalibrated to give a load of 500 mN. For the Waspaloy case, this method produced an unloading curve that was very close to the experimental curve. For P91, this method does improve the predicted unloading behaviour, but the predicted, recalibrated unloading curve isn't quite as close to the experimental data.

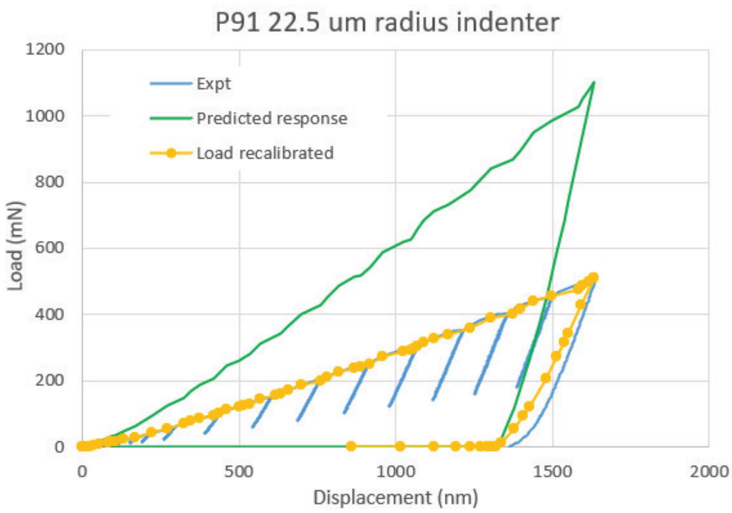

Figure 18 Experimental data compared to predicted load-displacement response from analysis with yield stress (A parameter) increased by a factor of 3 and the same data recalibrated to a load of 500 mN.

3.3 PARAMETRIC STUDY

The aim of the FEA modelling was to create a range of predicted load-displacement curves that could be used as training data. As a large number of curves are required to provide a large enough dataset, running the indentation FEA model as a parametric study is the most time efficient. The predicted data needed to be obtained from indentation into material with known properties.

During the material parameter calculations, Section 3.2.2, a hardening curve was obtained for both Waspaloy and P91. This was useful as a means of predicting indentation behaviour directly using experimentally measured tensile data. As discussed above in Section 3.2.1, using a single hardening curve for a material isn't ideal when running a parametric study designed to cover a range of different material properties. The modelling presented in Section 3.2.2 has demonstrated that the Johnson-Cook model provides very similar predictions. By using this material model, it is possible to run parametric analyses with varying model parameters and hence varying hardening behaviour.

The first step in setting up a parametric study was to define the parameters to be varied and the ranges to sweep the parameters across. When using the Johnson-Cook model, the Young's modulus and Poisson's ratio are required for the elastic definition. The hardening behaviour is then defined using Equation (15). As temperature effects are not included in the analysis, the terms $\hat{\theta}$ and m can be omitted, so only the parameters A, B and n are required to describe the hardening behaviour.

For both materials studied, the calculated Young's modulus, Poisson's ratio and parameter B were fixed, and the yield stress (A) and hardening exponent (n) were varied. It was necessary to ensure that the selected parameters produced a range of predicted force-displacement curves that enclose the experimental curves, especially the unloading curve, allowing for some material variability. The sections below describe the selection of the parameter ranges.

3.3.1 Waspaloy Parametric Ranges

For the Waspaloy material a series of FE models were run varying the A and n parameters, to investigate the effect of parameter variation on the unloading portion of the predicted load-displacement curve. Note that the A parameter value presented here takes into account a Tabor factor of 3 as described in Section 3.2.2 i.e. equivalent to 3 times the tensile yield stress. These predictions were compared to experimental data, with a selection of these curves shown in Figure 19. The loading curve is similar for all parameter sets, but the unloading curves provide a good range of unloading behaviour bounding the experimental data. Decreasing A shifts the predicted curve to the right as does increasing n.

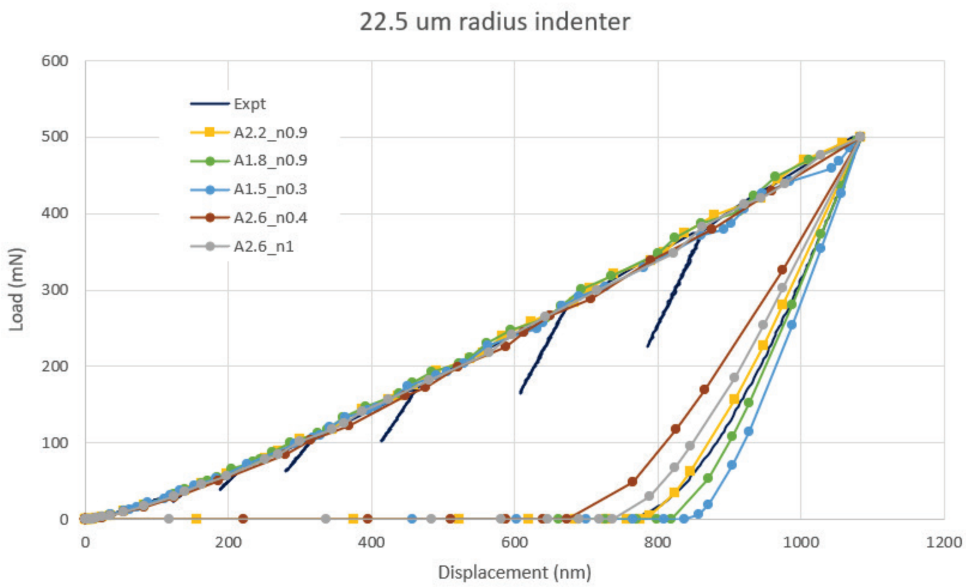

Figure 19 Predicted load-displacement curves, obtained from varying the A and n parameters in the Johnson-Cook model, compared with Waspaloy experimental data.

A set of over 150 curves was the minimum required for the training data, so a suitable number of A and n combinations was drawn up that consisted of 23 different A values and 7 different n values giving a total number of 161 predicted datasets. The following ranges were selected:

- Parameter A varying from 1.5 to 2.6 in 0.05 increments,
- Parameter n varying from 0.3 to 0.9 in 0.1 increments.

This A parameter range is equivalent to a tensile yield stress range of 0.5 GPa to 0.867 GPa. The range of hardening curves these parameter sets encompass are highlighted in Figure 20, where the hardening behaviour defined by the combinations of the minimum, mid and maximum values of A and n are used.

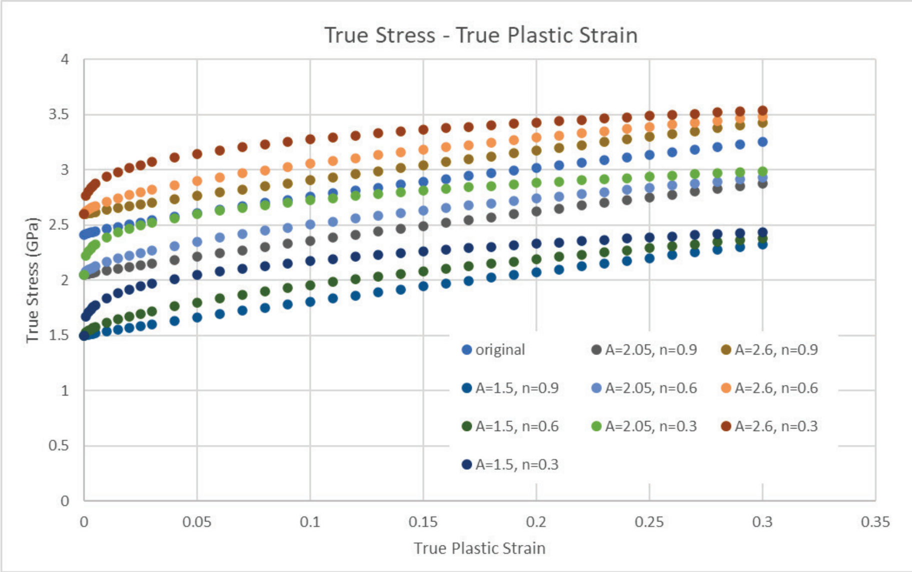

Figure 20 Hardening behaviour defined by the combinations of the minimum, mid and maximum values of A and n.

3.3.2 P91 Parametric Ranges

A series of FE models were also run for the P91 material, varying the A and n parameters, to determine suitable ranges for these parameters. Note that the A parameter value presented here accounts for a Tabor factor of 3 as described in Section 3.2.3, so the tensile yield stress would be a third of the input A parameter value. These predictions were compared to experimental data, with a selection of these curves shown in Figure 21. The loading curve is similar for all parameter sets, but the unloading curves provide a good range of unloading behaviour bounding the experimental data. Decreasing A shifts the predicted curve to the right as does increasing the parameter n.

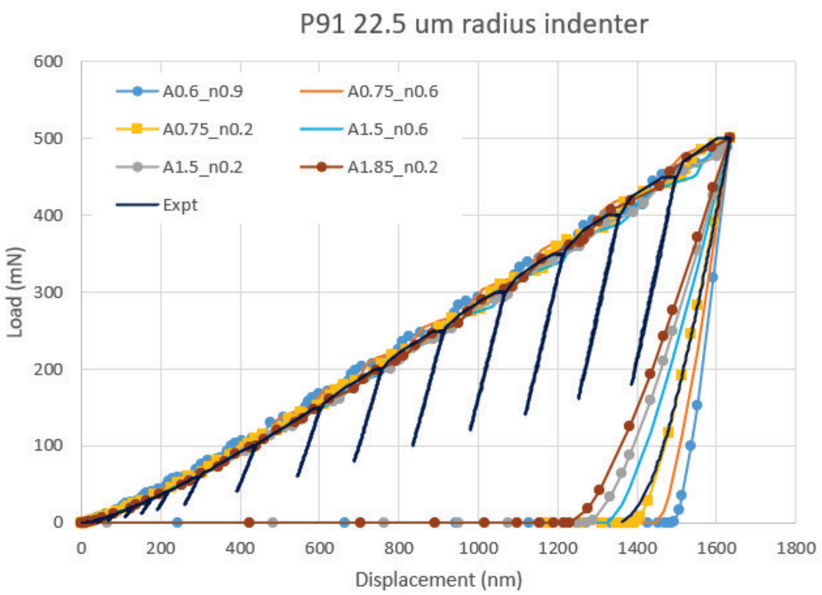

Figure 21 Predicted load-displacement curves, obtained from varying the A and n parameters in the Johnson-Cook model, compared with P91 experimental data.

To be consistent with the Waspaloy parametric study, a suitable number of A and n combinations was drawn up that consisted of 23 different A values and 7 different n values giving a total number of 161 predicted datasets. The following ranges were selected for P91:

- Parameter A varying from 0.6 to 1.7 in 0.05 increments,
- Parameter n varying from 0.2 to 0.8 in 0.1 increments.

This A parameter range is equivalent to a tensile yield stress range of 0.2 GPa to 0.567 GPa. The range of hardening curves these parameter sets encompass are highlighted in Figure 22, where the hardening behaviour defined by the combinations of the minimum, mid and maximum values of A and n are used.

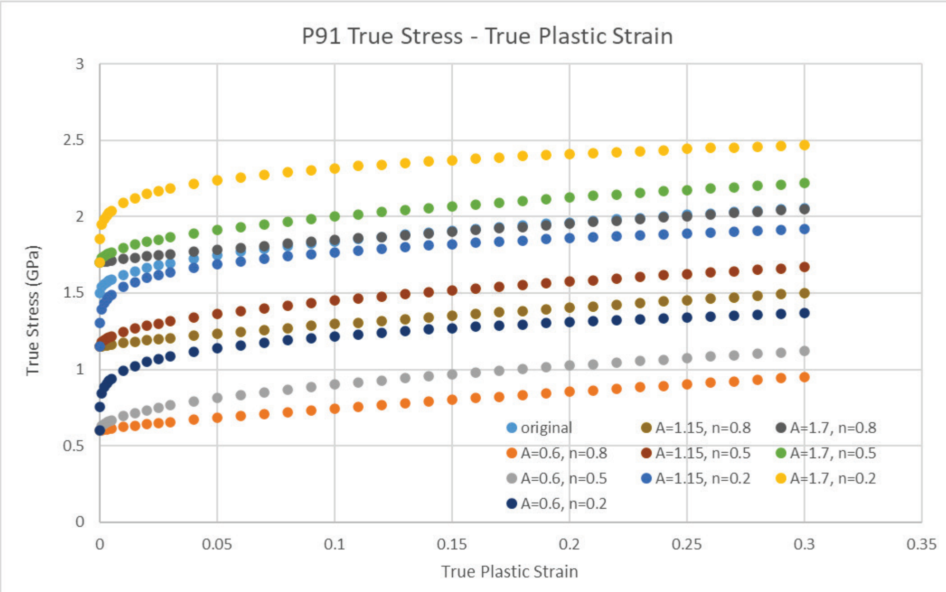

Figure 22 Hardening behaviour defined by the combinations of the minimum, mid and maximum values of A and n.

3.3.3 Running parametric analyses

A python script file can be used within Abaqus CAE to automate model generation and job submission. The indentation model described in Section 3.1 was used as the base model for the parametric study.

The python script file was used to set the Young's Modulus, Poisson's ratio, B parameter value and applied displacement. The applied displacement was obtained from the experimental indentation data and was 1634 nm for Waspaloy and 1083 nm for P91. The A and n parameters ranges selected above (Section 3.2.2) were input. The python script created a new input file for each possible combination of A and n parameters. To help with identification of the parameters used, the filenames created were of the form:

Job*x*_A*y*_n*z*

Where *x* is a sequential job number, *y* is the A parameter multiplied by 1000 (to ensure a whole number) and *z* is the n parameter multiplied by 10 for the same reason.

A csv file was also created which contained a list of all the jobs created plus the complete list of material parameters used for each job. A random selection of the input files had the applied displacement edited, to account for material variability as the experimental test runs to a set load rather than a set displacement. The python script then submitted the created jobs to run sequentially.

Once all the analyses were complete a second python script file was used within Abaqus CAE to open each output database file sequentially and output all the required results data. The requested data consisted of the vertical load and displacement from step 1 and 2, to produce the loading and unloading plot. The predicted deformation of the nodes along the top surface of the refined mesh region, under the indenter, was also output at the end of the loading and unloading steps.

This data, in the form of individual report files, was used as the training data for the neural network model discussed in Section 4.

4 REVERSE PROBLEM MODELLING

Inverse modelling is a method that can be used to try to infer bulk material tensile properties from indentation data. At its core, modelling the reverse problem is a multi-output regression problem. The inverse modelling problem was set up with yield stress σ_y and the hardening exponent n as the targets of the prediction model. Multi-output regression on these properties has been demonstrated before by researchers like Xia [6] and Lu [7].

As Section 4.1 will show, although the training FEA data was generated across a sweep of yield stress and n values, analysis shows it exhibits a lack of uniqueness. Lack of uniqueness is part of the general problem known as ill-posedness. Inverse problems such as in this case are frequently ill-posed and attempts to model them generally lead to numerically unstable predictions, extremely sensitive to the input (load-displacement curves in this case). This issue was highlighted by Lu [7], who noted that for a range of σ_y / n combinations, shifts to either parameter manifest in identical changes to loading curves, making it impossible to infer a unique combination of σ_y and n.

In the interest of understanding this issue in greater depth, more attention has been devoted to analysis of the features generated in the feature engineering step, Section 4.1. These tools should help diagnose the potential issues at an earlier stage.

4.1 FEATURE ENGINEERING

Feature engineering is comprised of three stages. Data cleaning, curve fitting and feature extraction. These are discussed in Sections 4.1.1 to 4.1.3 below.

4.1.1 Data Cleaning

Data cleaning is only essential when parsing experimental data, as FEA data is generally idealised. Experimental data in the form of multiload curves is processed differently than non-multiload tests.

In the case of the multiload curves, the approach taken was to sub-sample the loading curve by keeping a single data point from each loading period. This removes the data associated with tip retraction, which is necessary for further processing. Results are shown in Figure 23.

In the case of non-multiload curves, experimental data features a period of dwell at the peak load, leading to plastic relaxation. This relaxation behaviour is not present in FEA data, nor the models in reviewed literature and should be ignored. The cleaning algorithm detects the dwell region and removes it, shifting the unloading curve by the length of the 'shelf' to create continuity with the end of the loading curve. This is shown in Figure 24.

In all cases, the data loading functions were designed to work on raw text-based FEA and indentation output files. On loading, data is split into loading and unloading sections. Multiload experiment data was used in the following study, as FEA data was generated to match the displacement seen in multiload tests.

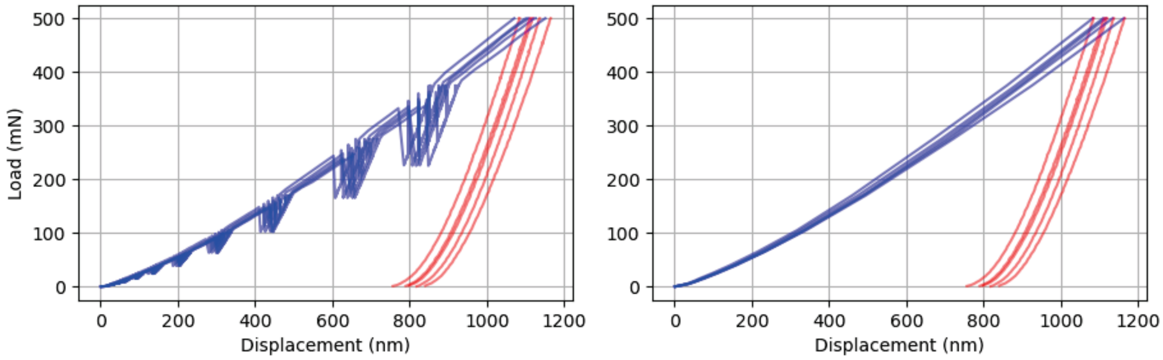

Figure 23 P91 experimental data showcasing multiload test retreat cleaning.

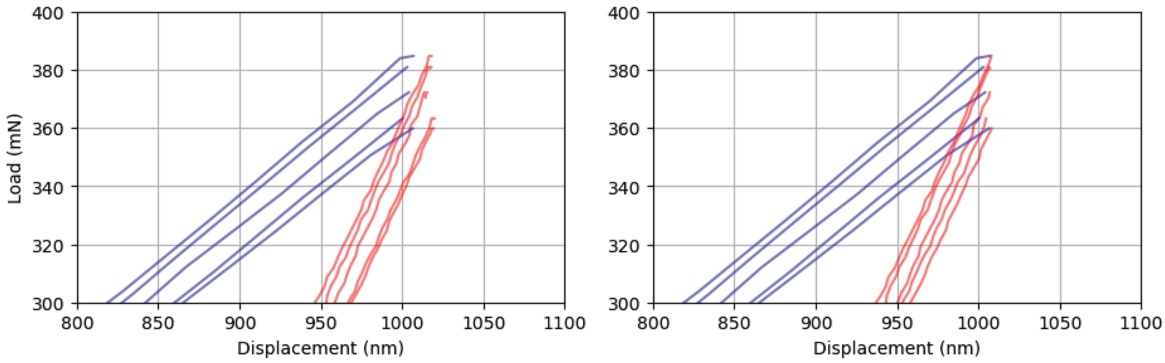

Figure 24 P91 experimental data showcasing dwell time compensation.

4.1.2 Curve Fitting

Curve fitted to the load/displacement data becomes the basis of extracting features based on gradients, integrals etc. Example curve functions found in literature used quadratic curves when loading with conical tip, but spherical tips produce curves with a significant linear component and are better captured with linear-quadratic equations, seen in Xia [6]. Adopting linear-quadratic equation would constrain the model too much, potentially removing important signal characteristics. For increased flexibility, a cubic spline model was adapted with a preset number of knot points. Using a cubic spline instead of a simpler quadratic spline ensures continuity of the second derivative, improving feature extraction. This approach is flexible enough that the same fitting algorithm is applied to loading and unloading curve sections, unifying the curve fitting and feature extraction algorithms. The structure of the fitted spline follows the pattern of using four ‘knots’ as illustrated in Figure 25. Knot #1 is placed a fraction of total displacement before knot #2. The role of knot #1 is to capture the curve’s tangency to the x axis. Knot #2 always has the x-position of the x-intercept. Knot #4 always has the x-position of the maximum displacement. Knot #3 is automatically positioned by the fitting algorithm to minimise the fitting error.

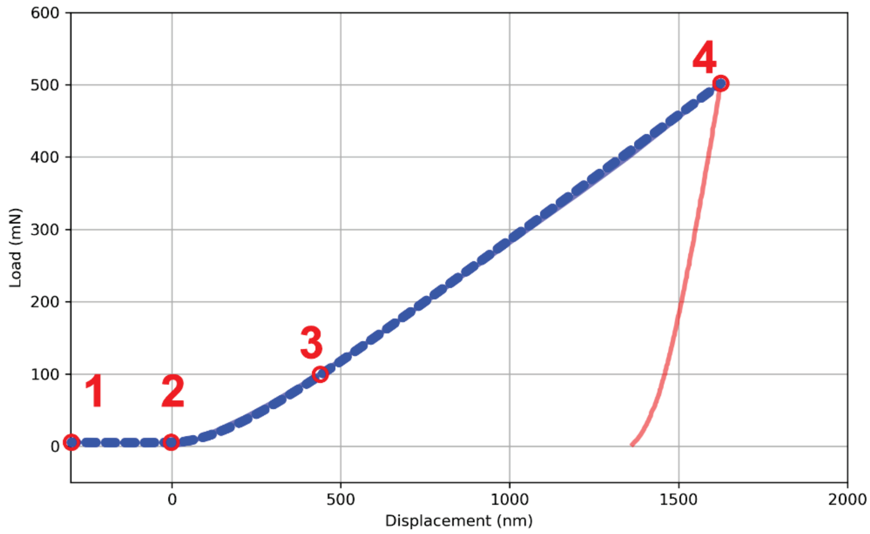

Figure 25 Structure of fitted cubic spline using four knots.

4.1.3 Feature Extraction

The process of feature extraction aims to produce a small number of descriptive features of the observed data and is specific to the data analysed. In tests with a conical indenter, the loading part of the load-displacement curve can be approximated by a quadratic equation. However, the spherical indenter used in this work produces a loading profile strongly approximating linear, especially towards the end of loading process.

Work type features were calculated through numerical integration of the loading/unloading splines, from x-intercept to intersection point of the curves. Normalized type features were calculated as standard, with the step of normalizing the load/displacement values to a 0-1 range. Curvature type features were calculated as second derivative of the cubic splines at the third knot location.

The following features were computed, see Figure 26:

1. **Unloading Slope S_U**: The slope of the unloading curve calculated using a spline fit.
2. **Loading Slope S_L**: The slope of the loading curve calculated using a spline fit.
3. **Normalized Unloading Slope S_{UN}**: The slope of the unloading curve after normalizing the data.
4. **Normalized Loading Slope S_{LN}**: The slope of the loading curve after normalizing the data.
5. **Elastic Work (W_e)**: The elastic work done during the indentation process.
6. **Plastic Work (W_p)**: The plastic work done during the indentation process.
7. **Elastic Work Fraction: W_e / (W_e+ W_p)**.
8. **Displacement Ratio**: The ratio of final to maximum displacement h_r / h_m
9. **Loading Curvature**: The second derivative at knot #2

It was reasoned that the values of displacement, load and work must only be used as dimensionless ratio, as their absolute values depend mainly on the test's maximum load/displacement and are therefore a function of test design, not the tested material intrinsically. Therefore, elastic work and plastic work features were removed from the feature set, leaving only the work ratio.

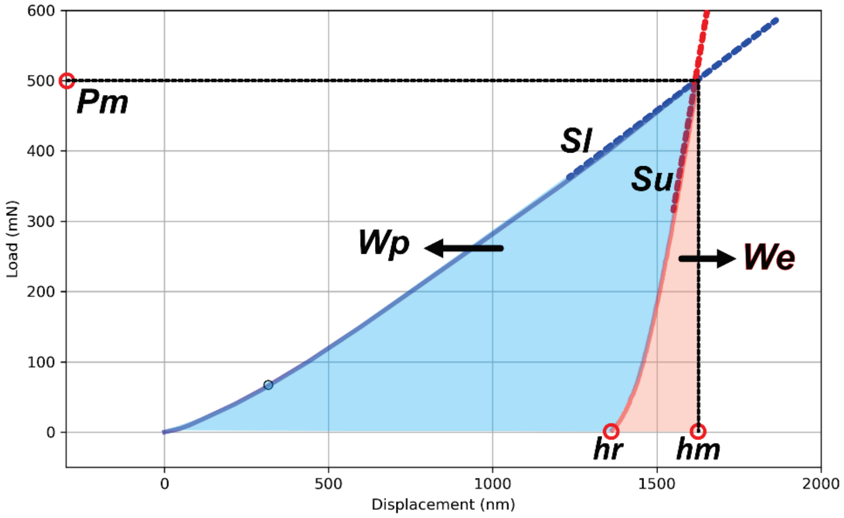

Figure 26 Illustration of features extracted from loading curves.

4.2 MODELLING APPROACH

4.2.1 Feature Inspection

All features are extracted from the load-displacement curve. Similar curves should produce similar features to arrive at a stable regression model. The similarity metric used to compare the features is Euclidean distance between the feature vectors. When FEA data is clustered based on similarity, highly disparate combinations of n and σ_y produce curves which are virtually indistinguishable. Figure 27 (a) shows a set of clusters with highest self-similarity. The same clusters are plotted on the σ_y vs n grid, to visualize the combination of properties producing each cluster, Figure 27 (b). This illustrates that any model fitted to this data will struggle to produce a unique combination of σ_y and n. Given the spacing and linear relationship between n and σ_y in the grid in Figure 27 (b), it is expected that the samples in the upper left and lower right of the grid will not have fewer or no corresponding similar curves present in the dataset. This has potential to introduce false confidence in a small set of data with unique property combination.

(a)

(b)

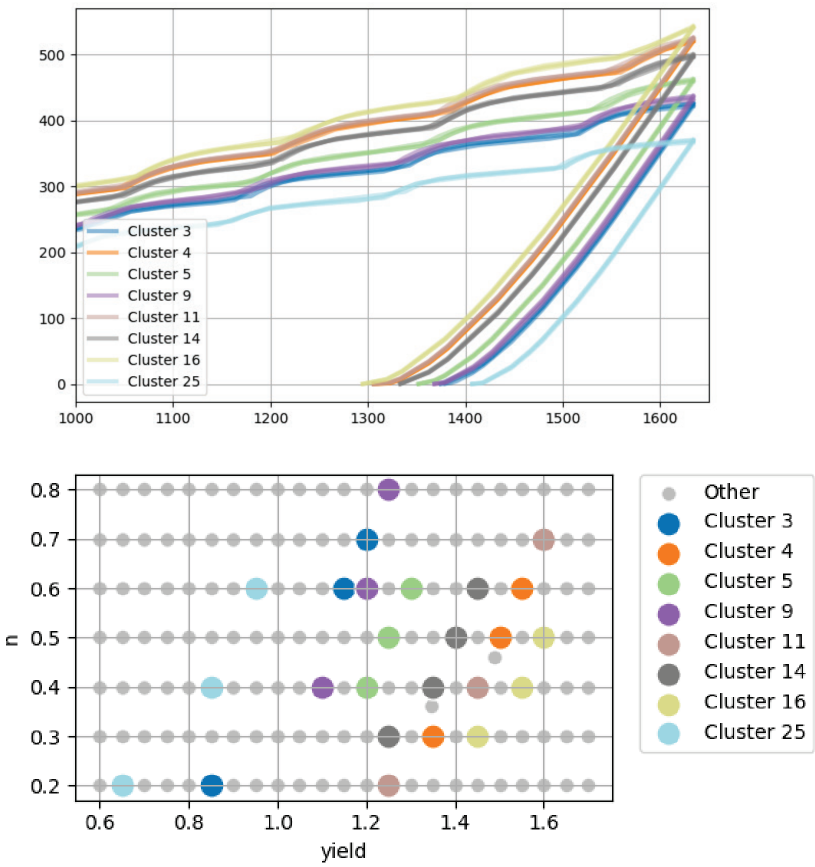

Figure 27 (a) a subset of P91 FEA load/displacement curves, clustered by similarity. Each cluster contains at least 3 overlapped curves. (b) the same set of clusters, displayed on the grid of FEA simulated σ_y and n values.

FEA data load was scaled by a factor to match experimental data. To find the scaling factor, a feature distance metric was used to minimise the mean distance between experimental curves and the FEA curve produced with matching mechanical properties. This process initially produced poor overlap between FEA and experimental data. This is because the approach of scaling the load is not sufficient to align all features of the curve. For example, matching the slope of loading section leads to mismatch in unloading slope and vice-versa.

To produce a reasonable overlap, we produced a best-match using only two features - loading slope and plastic work. A consequence of this mismatch is that attempting to use the FEA-trained model for inference on experimental data could produce erroneous results. To quantify this similarity, a feature vector distance metric (KNN, K-nearest neighbours analysis) was used. Figure 28 charts all P91 FEA curves compared against one experimental curve. Four FEA curves nearest to experimental in the feature space are highlighted. Only the first neighbour has approximately the same loading slope as the experimental. The three remaining neighbours appear to have approximately the same unloading slope, but greatly smaller loading slope.

When all features are taken into account simultaneously, experimental data is dissimilar from FEA data. This can be further quantified with the distance metric. For any FEA curve, the average distance to its four closest neighbours is 0.3203 (dimensionless). For any experimental curve, the average distance to four nearest FEA curves is 9.6909. This solidifies the conclusion that inference on experimental data is unlikely to be successful.

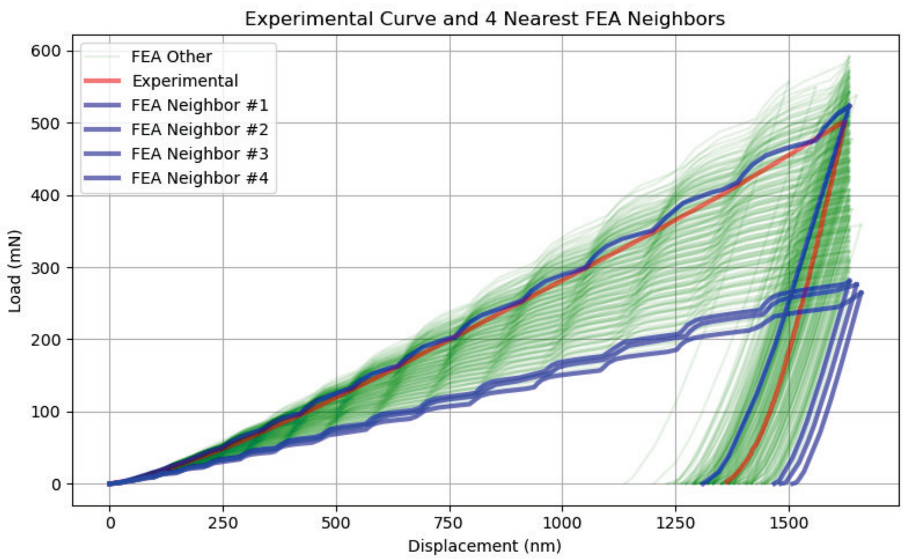

Figure 28 Comparison of experimental loading curve against FEA curves, with results of KNN analysis.

4.2.2 Model selection rationale.

At its core, modelling the reverse problem is a multi-output regression problem. Xia [6] and Lu [7] perform feature engineering which reduces the load-displacement curves to fewer than 10 features, making this a structured data problem. The number of samples in the training set is less than 1000. Based on those rough estimates, Gradient Boosting (GB) was chosen as the modelling approach, rather than the neural networks implemented by Xia [6] and Lu [7]. Specifically implemented in XGBoost library, Gradient Boosting methods have the following advantages:

- Computational Efficiency- GB models can be trained rapidly, including on CPU when GPU is not available. This is especially useful at early development stage where hundreds of training attempts can be used to find optimal hyperparameters.
- GB models perform very well on the medium-sized datasets as used in this case.
- GB models offer interpretability of feature importance, while obtaining feature important metrics in Convolutional Neural Network (CNN) models is more challenging.
- XGBoost library specifically is well documented and easy to implement.
- Given the small number of features, GB is able to potentially capture complex relationships between features.

4.2.3 Model Regularization- Hyperparameter Tuning on Augmented Data

The FEA data was generated using combinations of yield stress (σ_y) and n populating a dense grid, as shown in Figure 29 (a). During initial regression tests, it was found that this regular spacing was conducive to model overfitting. That is, given the limited number of unique answers, a machine learning model of sufficient complexity could 'memorize' the target values, giving it very high performance on training, but very low performance on unseen validation data. Regularization steps were needed to prevent that.

Firstly, a data augmentation step was implemented where small amount of variance is added to the FEA ground truth values of yield strength, σ_y, (2%) and n (4%). To further reduce overfitting, noise was added to the features collected from FEA curves, Figure 29 (b). For each feature, the standard deviation of applied noise was based on standard deviation observed in experimental data curves. The noise-free data and ten versions of FEA dataset with normal noise were stacked into larger dataset, which was then used for hyperparameter tuning.

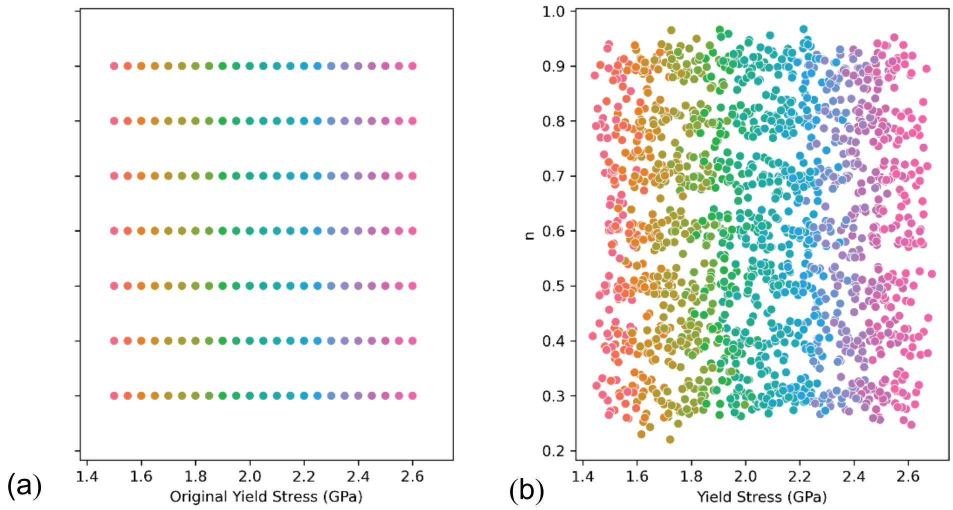

Figure 29 P91 data augmentation through noise injection.

XGBoost algorithm exposes a large number of hyperparameters which affect its training behaviour in regard to the model complexity and overfitting mitigation. When target variables (σ_y and n) are highly correlated as in this case, two common methods of regularization are used: Ridge regression (also called Tikhonov regularization or L2 regularization) and Lasso regression (or L1 regularization). Combination of both methods is referred to as elastic net regression. In XGBoost, reg_alpha controls the strength of L1 regularization, reg_lambda controls the strength of L2 regularization. To find optimal combination of these regularization methods, we decided to adapt a python package Optuna, which provides an algorithm for searching the defined hyperparameter space using Bayesian process. Multiple optimization runs were performed on both Waspaloy and P91 datasets. The range of tested values and the final optimisation results for both materials are shown in Table 6.

Table 6 XGBoost Hyperparameter search results.

Hyperparameter	Type	Range	Scale	Optimisation result
max_depth	Integer	4 to 9	Linear	8
n_estimators	Integer	200 to 1000	Linear	838
colsample_bytree	Float	0.1 to 1.0	Linear	0.9684
learning_rate	Float	1e-3 to 0.2	Log	0.0144
min_child_weight	Integer	1 to 10	Linear	4
reg_alpha	Float	1e-3 to 10.0	Log	0.0012
reg_lambda	Float	1e-3 to 10.0	Log	3.62477

4.2.4 Model Final Training and Fitting Results for Waspaloy and P91

The hyperparameters obtained through tuning on noisy data were the ones used to train a new model, using only the noise-free original data. A random 20% subset of FEA data was held out during training for final validation. Additionally, during the design of FEA simulations, a small subset of simulations were performed where the setpoint displacement was changed from nominal 1500nm to values above and below that displacement. We reasoned that a well-tuned model should not be sensitive to the value of maximal displacement, as this value is a feature of experiment design, not the material intrinsically. The curves with altered ultimate displacement were also set aside for validation.

For the P91 material four plots are provided below, comparing true vs. predicted independent variables. Figure 30 shows the results for test/train dataset. Figure 31 shows the results for holdout validation set. Figure 32 presents the results for alternative displacement validation set. For completeness, Figure 33 is the inference on experimental data. Datapoints are coloured according to the scale of the other independent variable i.e. colour of points in yield strength plot is a function of hardening exponent and vice-versa. This visualisation was used for identifying potential model biases e.g. if high hardening would lead to over-estimation of yield strength. Random distribution of colour indicates lack of systematic bias, which is a positive indicator of model quality.

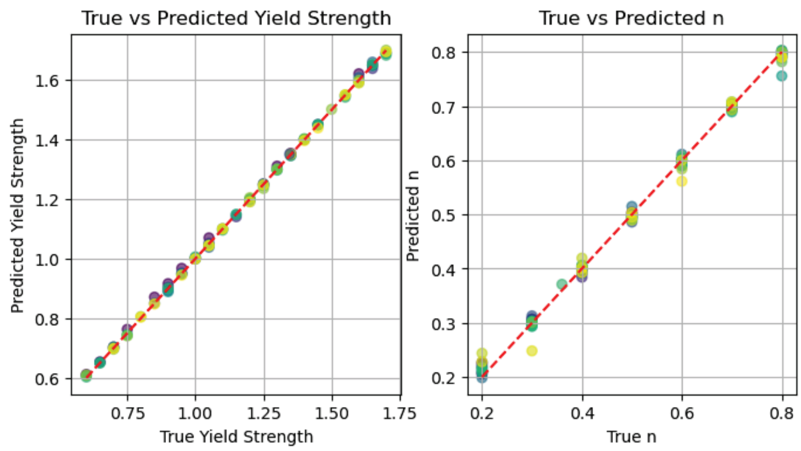

Figure 30 Model predictions on P91 test/train set.

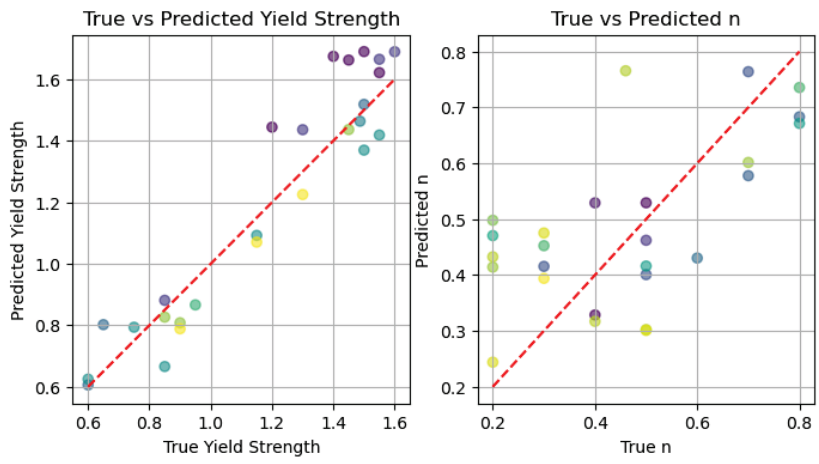

Figure 31 Model prediction on P91 holdout validation set.

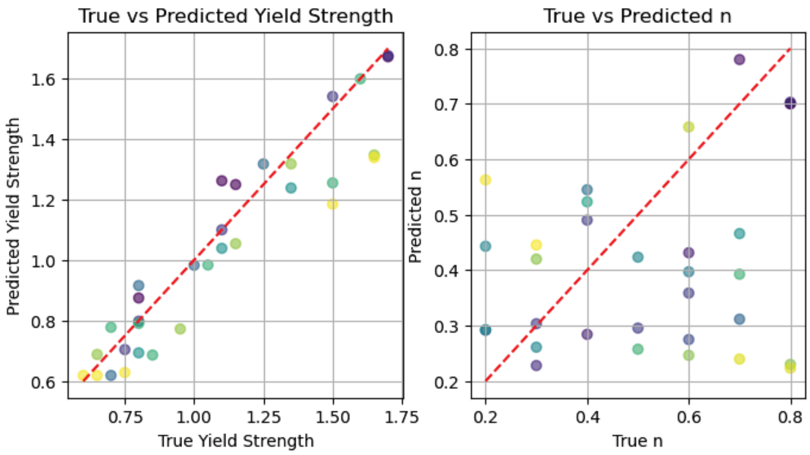

Figure 32 Model predictions on P91 alternative displacement validation set.

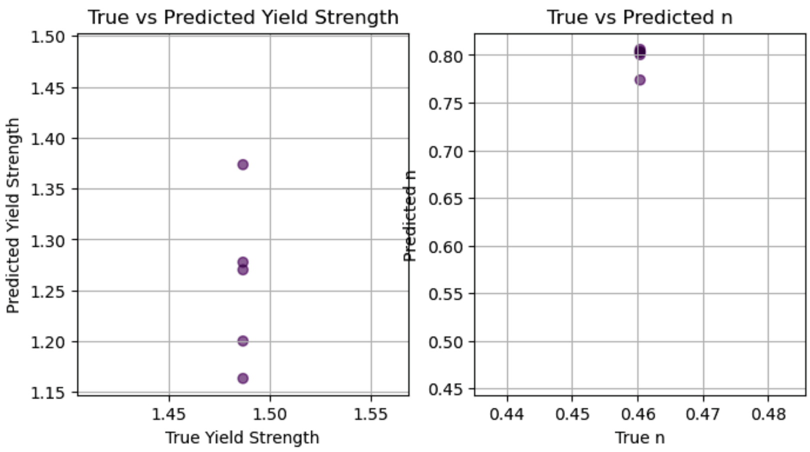

Figure 33 Model predictions on P91 experimental data.

For the Waspaloy material four plots are provided below, comparing true vs. predicted independent variables. Figure 34 shows the results for test/train dataset. Figure 35 shows the results for holdout validation set. Figure 36 presents the results for alternative displacement validation set. For completeness, Figure 37 is the inference on experimental data. As before datapoints are coloured according to the scale of the other independent variable i.e. colour of points in yield strength plot is a function of hardening exponent and vice-versa.

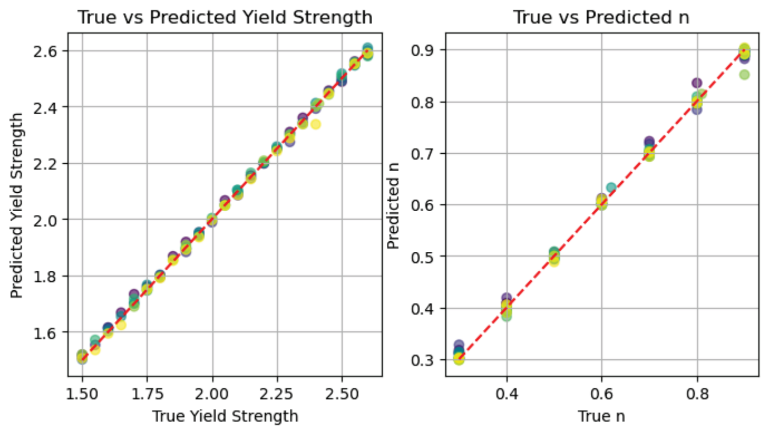

Figure 34 Model predictions on Waspaloy test/training set.

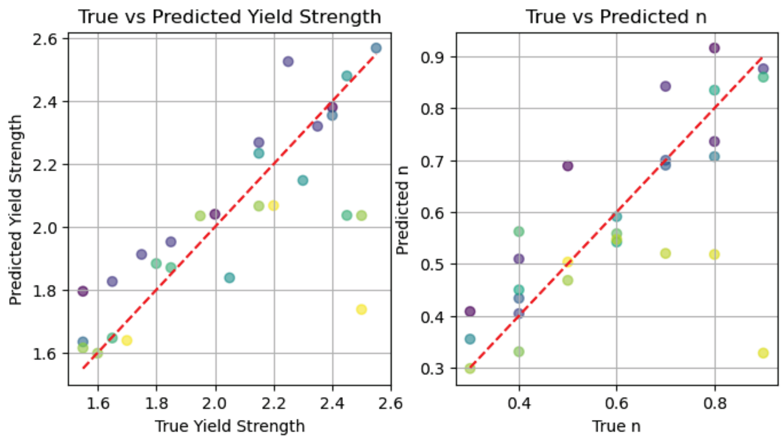

Figure 35 Model predictions on Waspaloy holdout validation set.

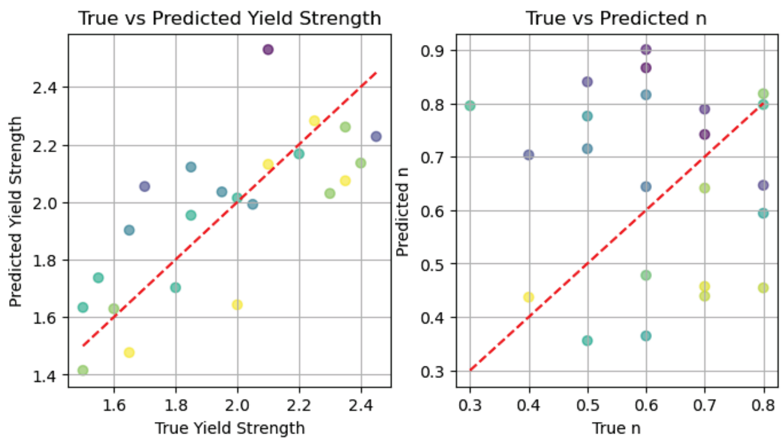

Figure 36 Model predictions on Waspaloy alternative displacement validation set.

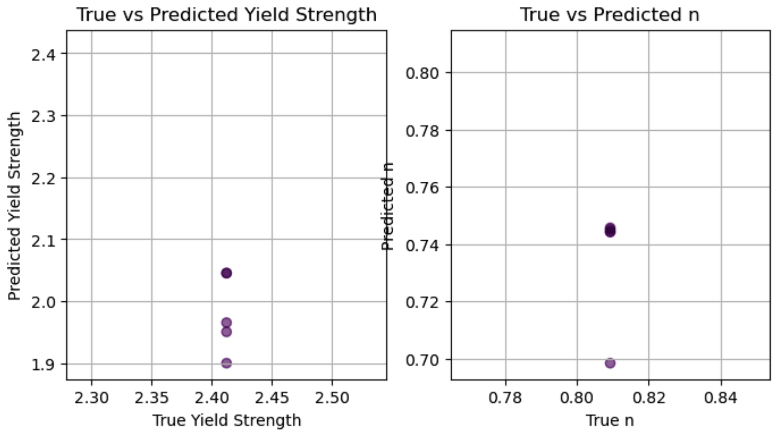

Figure 37: Model predictions on Waspaloy experimental data set.

4.2.5 Results Summary

For both simulated materials, the same set of conclusions can be drawn.

1. The fit to the test/training set is highly accurate, which is not the expected result, following the discussion on the non-uniqueness of the loading curves. It is believed that despite the effort to prevent overfitting through normalization and noise injection, the nature of the FEA dataset still allows the model to overfit.
2. Overfitting is confirmed through much poorer result on the holdout data. While some inference can be made on independent variable scale, the predictions are highly uncertain and the accuracy is lower for hardening exponent. This is expected, since as can be seen in Figure 27, clusters of similar curves have larger range of n than σ_Y.
3. The inference results on alternative displacement set are similar to the holdout validation for σ_Y, but accuracy of n prediction is notably less. It indicates that despite the rationale applied to feature selection, the features are still sensitive to the final stopping conditions of the test. This indicates that the model should be trained on and used only on data with specific load/displacement limits for accurate inference.
4. The amount of experimental data available is insufficient to make informed comments on the performance of the model on real data. A notable aspect of the inferred hardening exponent especially is that regardless of accuracy, the spread of predictions is much less than in FEA data. This is not an indication of modelling precision. Rather, based on the discussion of feature vector space, it is thought that the experimental data is so dissimilar to FEA data that it exists well outside of the modelled behaviour, in a ‘flat’ space where features are not correlated with outputs.

5 CONCLUSIONS

Several methods were used and analysed to extract strain-stress data from multiple load-displacement curves. For P91 and Waspalloy, tabor strain and stress with strain related to a/R were found to work better with the current setting. The results demonstrate that it’s challenging to make meaningful measurements of yield strength with existing models to convert the indentation strain stress data to Tabor strain stress for Waspaloy, while the Young’s Modulus and yield stress data collected from the P91 fit reasonably well to experimental tensile data. This was attributed to that P91 fit work hardening law, which is the assumption of the indentation models. For Wasploy, via Hertz fit, the initial maximum shear stress was calculated to be about 1.4 GPa, which is much higher than the tensile yield strength. This has been shown to be the case from other indentation measurement methods, therefore, a more complex model should be developed to be representative of the complex work hardening behaviour of Waspaloy.

The inverse modelling problem was set up with yield stress σ_y and the hardening exponent n as the targets of the prediction model. However, our simulation dataset presented unique challenges. The first limitation stemmed from the misalignment between FEA loading curves and the experimental loading curves. The fit may be made approximately correct by applying a load scaling factor, but as discussed in Section 4.1, this was not sufficient to create a correspondence between FEA and experimental data. The second limitation stemmed from lack of experimental data covering a range of mechanical properties. For both P91 and Waspaloy the experimental data was obtained on a single representative material sample. This meant it was not possible to test regression on experimental data. The third limitation was the lack of solution uniqueness. This issue was highlighted by Lu [7], who noted that for a range of σ_y / *n* combinations, shifts to either parameter manifest in identical changes to loading curves, making it impossible to infer a unique combination of σ_y and *n*. Inverse problems such as in this case are frequently ill-posed and attempts to model them generally lead to numerically unstable predictions, extremely sensitive to the input (load-displacement curves in this case). As a result, attempts to train a regression model did not yield satisfactory results. It is not clear if the ill-posedness is an issue inherent to the physical process of microindentation at this scale, or if the issue is specific to current implementation of the FEA model. In interest of understanding this issue in greater depth, more attention was devoted to analysis of the features generated in the feature engineering step. The methods and code used in feature engineering and analysis will be useful in providing faster feedback in future attempts at solving the microindentation inverse problem.

6 REFERENCES

[1] D. Tabor, "Indentation hardness: Fifty years on - A personal view," *Philosophical Magazine A,* vol. 74, no. 5, p. 1207–1212, 1996. https://doi.org/10.1016/S0040-6090(01)01439-0

[2] E. G. Herbert, W. C. Oliver and G. M. Pharr, "On the Measurement of Yield Strength by SPherical Indentation," *Philosophical Magazine,* vol. 86, p. 5521, 2006. https://doi.org/10.1016/S0040-6090(01)01439-0

[3] J. D. Morrow and F. R. Tuler, "Low Cycle Fatigue Evaluation of Inconel 713C and Waspaloy," *J. Basic Eng.,* vol. 87, p. 275, 1965.

[4] A. Ruiz-Moreno, P. Hahner, F. Fumagalli, V. Haiblikova, M. Conte and N. Randall, "Stress-Strain Curves and Derived Mechanical Parameters of P91 Steel from Spherical Nanoindentation at a Range of Temperatures," *Materials & Design,* vol. 194, p. 108950, 2020. https://doi.org/10.1016/j.matdes.2020.108950

[5] Abaqus FEA Software, *©2009-2021, Dassault Systèmes Simulia Corp..*

[6] J. Xia, C. Won, H. Kim, W. Lee and J. Yoon, "Artificial Neural Networks for Predicting Plastic Anisotropy of Sheet Metals Based on Indentation Test," *Materials,* vol. 15, p. 1714, 2022. https://doi.org/10.3390/ma15051714

[7] L. Lu, M. Dao, P. Kumar, U. Ramamurty, G. E. Karniadakis and S. Suresh, "Extraction of mechanical properties of materials through deep learning from instrumented indentation," *Proceedings of the National Academy of Sciences (PNAS),* vol. 117, no. 13, pp. 7052-7062, 2022. https://doi.org/10.1073/pnas.1922210117